Complement Decay-Accelerating Factor is a modulator of influenza A virus lung immunopathology

Nuno Brito Santos[1,6], Zoé Enderlin Vaz da Silva[1,6], Catarina Gomes[2,3], Celso A. Reis[2,3,4,5] and Maria João Amorim[1,*]

[1]Cell Biology of Viral Infection Lab, Instituto Gulbenkian de Ciência, Oeiras, Portugal

[2]Instituto de Investigação e Inovação em Saúde (i3S), University of Porto, 4200-135 Porto, Portugal

[3]Institute of Molecular Pathology and Immunology of the University of Porto (IPATIMUP), 4200-135 Porto, Portugal

[4]Molecular Biology Department, Institute of Biomedical Sciences of Abel Salazar (ICBAS), University of Porto, 4050-313 Porto, Portugal

[5]Pathology Department, Faculty of Medicine, University of Porto, 4200-319 Porto, Portugal

[6]These authors contributed equally

*Corresponding author

Tel: + 351 214407905

Fax: + 351 214407970

Email mjamorim@igc.gulbenkian.pt

Short Title: Decay-Accelerating Factor and influenza A virus immunopathology

Abstract

Clearance of viral infections, such as SARS-CoV-2 and influenza A virus (IAV), must be fine-tuned to eliminate the pathogen without causing immunopathology. As such, an aggressive initial innate immune response favors the host in contrast to a detrimental prolonged inflammation. The complement pathway bridges innate and adaptive immune system and contributes to the response by directly clearing pathogens or infected cells, as well as recruiting proinflammatory immune cells and regulating inflammation. However, the impact of modulating complement activation in viral infections is still unclear. In this work, we targeted the complement decay-accelerating factor (DAF/CD55), a surface protein that protects cells from non-specific complement attack, and analyzed its role in IAV infections. We found that DAF modulates IAV infection *in vivo,* via an interplay with the antigenic viral proteins hemagglutinin (HA) and neuraminidase (NA), in a strain specific manner. Our results reveal that, contrary to what could be expected, DAF potentiates complement activation, increasing the recruitment of neutrophils, monocytes and T cells. We also show that viral NA acts on the heavily sialylated DAF and propose that it exacerbates complement activation, leading to lung immunopathology. Remarkably, this mechanism has no impact on viral loads but rather on the host resilience to infection and may have direct implications in zoonotic influenza transmissions.

Author summary

Exacerbated complement activation and immune deregulation are at the basis of several pathologies induced by respiratory viruses. Here, we report that complement decay-accelerating factor (DAF), which inhibits complement activation in healthy cells, increases disease severity upon Influenza A virus (IAV) infection. Remarkably, DAF

interaction with IAV proteins, hemagglutinin (HA) and neuraminidase (NA), resulted in excessive complement activation and recruitment of innate and adaptive immune cells, without affecting viral loads. Furthermore, we observed that viral NA directly cleaves DAF and promotes complement activation, providing a possible link between IAV-DAF interaction and pathology. Therefore, our results unveil a novel pathway that could modulate disease severity, which may help to understand the increased pathogenicity of zoonotic and pandemic IAV infections.

Introduction

Host-pathogen interactions are very complex with both parts contributing to the progression and outcome of infections. In the case of viruses, pathogen- and damage-associated molecular patterns (PAMP and DAMP, respectively) are detected by pattern recognition receptors (PRR) alerting the host of their presence, and triggering the immune response to clear the infection (1,2). It is generally accepted that for viral infections, an aggressive initial activation of innate immunity favors the host, whilst mechanisms that originate prolonged inflammation are associated with severe outcomes. This paradigm underpins for example the sex differences observed for coronavirus disease 19 (COVID-19), that results in lower death rate in women, despite similar incidence of infection in both sexes (3–5). However, an excessive immune response activation might destabilize the equilibrium needed to eliminate the pathogen without causing tissue damage, and lead to immunopathology (6,7). It is therefore important to determine the host factors and viral characteristics that result in an efficient immune response for clearing the pathogen without provoking immunopathology.

Influenza A virus (IAV) is the prevalent cause of seasonal flu, a relevant health problem as it kills up to 600,000 people worldwide yearly (8). IAV replication occurs in the upper and lower respiratory tract, peaks normally 2 days after infection, and in most cases little virus shed can be detected after 6 days. For the majority of people, symptoms (fever, cough, acute viral nasopharyngitis, headache) clear after 7-10 days, with fatigue enduring for weeks, without serious outcomes (8–10). In a proportion of people, however, severe complications occur, with the elderly, immunosuppressed, pregnant women, and people with associated comorbidities being at higher risk (11). IAV can also provoke pandemic outbreaks, associated with zoonotic events, which lead to significant higher mortality than seasonal epidemics. The 1918 Spanish influenza, for example, caused up to 50 million

deaths (12). Complications may include hemorrhagic bronchitis, pneumonia (primary viral or secondary bacterial), and death (13–16). They usually derive from an exacerbated immune response leading to tissue damage (17,18). Identifying intrinsic risk factors that contribute to severe disease outcomes may minimize immunopathology in the lungs and uncover new therapeutic targets with decreased proneness to develop resistance.

Defects in type I IFN response have been associated with the more severe cases of COVID-19 (19,20), suggesting that the initial steps in immune activation define disease outcome. However, there are other players involved in mounting immune responses, such as the complement system. The complement system has been extensively reviewed (21–23) and consists in a cascade of proteolytic interactions that lead to the direct killing of the pathogen or infected cell, as well as proinflammatory immune cell recruitment. Remarkably, C3 has been found within the mucus barrier (24), which elucidates complement role in early immune response upon pathogen infection in the airways. Disease severity and mortality have been associated with both lack or excess of complement activation in several viral infections such as Severe Acute Respiratory Syndrome Coronavirus (SARS-CoV) (25,26), Middle Eastern Respiratory Syndrome Coronavirus (MERS-CoV) (27), SARS-CoV-2 (28–30), and IAV (31–33). However, it is still unclear how fine-tuning complement activation may impact in the development of disease severity. One strategy to tune complement activation in infection is to target its regulators. Complement decay-accelerating factor (DAF/CD55) is a membrane-bound regulator of complement activation (RCA) exposed at the surface of most cell types, including human and murine airways (34–36). DAF promotes the decay of C3 convertases, thus protecting healthy cells from non-specific complement attack, and inhibiting the release of anaphylatoxins that would recruit and activate the immune response (37–39). In humans, it has been reported that DAF deficiency leads to excess complement activation with systemic implications (40,41). Furthermore, SNPs in DAF promoter region decreasing

111 protein expression have been associated with higher risk of severe infections by pandemic
112 and avian IAV strains (42,43).

113 In this work, we explore the role of DAF in activating complement and in
114 modulating IAV infection via an interplay with the antigenic viral proteins hemagglutinin
115 (HA) and neuraminidase (NA). We observed that DAF, contrary to what could be
116 expected, potentiates complement activation in IAV infection. We also describe that viral
117 NA acts on DAF, in a strain-specific manner, removing α-2,6-linked sialic acids and
118 propose that this may influence pathogenicity. Given that the recognition of different
119 conformations of sialic acid by the influenza virus is a key driver in influenza intra- and
120 interspecies transmission, our findings may have implications for zoonotic events. Our
121 results also showed that DAF leads to increased complement activation, as well as
122 immune cell recruitment, especially of neutrophils and monocytes, increasing lung
123 immunopathology without altering viral loads. Our work reveals a novel mechanism of
124 virulence in IAV infection.
125

Results

Decay-accelerating factor (DAF) aggravates IAV infection by increasing immunopathology.

Immune response to viral infections such as IAV must be tightly regulated in order to clear the pathogen without causing immunopathology. The complement system is at the frontline of the immune response, recognizing pathogens, and activating and recruiting immune cells. The absence of a regulator of this system, such as DAF, is expected to increase complement activation, resulting in more efficient viral clearance and/or increased tissue damage. To assess the consequences of DAF depletion in the context of IAV infection, C57BL/6J (WT) and C57BL/6J *Daf*$^{-/-}$ (*Daf*$^{-/-}$) mice were challenged with two different H1N1 strains circulating in the human population: A/California/7/2009 (Cal) and A/England/195/2009 (Eng). For each viral strain, we measured bodyweight loss, as proxy for disease severity, and followed survival up to 11 days post infection (d.p.i.) (Fig. 1). Surprisingly, we observed that upon infection with Cal, *Daf*$^{-/-}$ mice exhibited reduced bodyweight loss starting at 4 d.p.i., when compared to the WT, and maintained that difference throughout the experiment (Fig. 1-A). In addition, percentage of survival of *Daf*$^{-/-}$ mice when infected with Cal was higher than of WT mice (75% vs. 25%) (Fig. 1-B). Similarly, upon challenge with Eng, *Daf*$^{-/-}$ mice had increased survival (50% vs. 25%), but lost more of their initial bodyweight when compared to the WT (Fig. 1-C, D). WT mice surviving to Eng infection had a milder bodyweight loss when compared to *Daf*$^{-/-}$ mice, thus explaining the reversion in trends later in infection, and the consequent discrepancy between bodyweight loss and survival. Taken together, our data indicate that DAF exerts a detrimental effect for the host during IAV infection.

We then extended the observation to two different well-characterized IAV strains: the mouse adapted virulent H1N1 A/Puerto Rico/8/1934 (PR8) and the less virulent H3N2 A/X-

31 (X31). X31 is a reassortant strain of PR8 containing segments 4 and 6 from A/Hong Kong/1/68 (HK68) (44) and for clarity purposes, the X31 strain will be mentioned as PR8-HK4,6 throughout this work. WT and *Daf*$^{-/-}$ mice were infected with sublethal and lethal doses of PR8 or PR8-HK4,6, and bodyweight loss and mortality assessed for 11 d.p.i.. Upon infection with PR8, *Daf*$^{-/-}$ and WT mice presented similar bodyweight loss and all mice succumbed to the disease, *Daf*$^{-/-}$ mice at 7 d.p.i., and WT mice at 8 d.p.i. (Fig. 2-A, B). Upon infection with PR8-HK4,6, as observed in infections with the circulating strains, *Daf*$^{-/-}$ mice had a less severe disease and mortality when compared with their WT counterparts. These mice lost less of their initial bodyweight (-11.3% vs. -20.4%) and had reduced mortality than WT mice (50% vs. 100%) (Fig. 2-C, D). The discrepancy between PR8 and the other strains might be explained by the high virulence of this strain where 500 PFU of PR8 are a lethal dose, here quantified by the humane endpoint of infection of a loss of more than 25% of initial bodyweight. These results show that DAF worsens disease outcome in infection with mildly virulent IAV strains, both circulating in the human population and lab-adapted but not with more virulent IAV strain.

As DAF is a complement regulator, the results indicate a role for complement in modulating disease outcome. To dissect between the role of the complement pathway and of this particular molecule, C57BL/6J mice depleted of CD59 (*Cd59*$^{-/-}$), another regulator of complement activation (RCA), were infected with PR8-HK4,6, and bodyweight loss and mortality assessed for 11 d.p.i.. Interestingly, there was no difference in bodyweight loss and mortality between *Cd59*$^{-/-}$ mice and their WT counterparts, with all mice succumbing to the disease at 7 d.p.i. (Fig. 2-E, F). This indicates that the protection observed in *Daf*$^{-/-}$ mice is mediated by the absence of this particular RCA, and not due to a general complement deregulation.

Taken together, our results suggest a role for DAF in disease outcome. To further dissect the mechanisms behind such role, we focused on infections with PR8-HK4,6 as it is a well-described laboratorial model, with a virulence resembling circulating strains.

Protection conferred by DAF depletion could be explained by a decrease in viral burden or by preventing immunopathology (6). To distinguish between these two hypotheses, we started by assessing lung viral loads of WT and *Daf*$^{-/-}$ mice infected with a sublethal dose of PR8-HK4,6. Samples were collected at day 3 and 6 p.i. to distinguish between early viral replication and clearance. At both time points, lung viral titers were identical in WT and *Daf*$^{-/-}$ mice (3.8±2.8 x 10^6 PFU/g vs. 3.1±2.7 x 10^6 PFU/g at 3 d.p.i., and 3.2±2.7 x 10^5 PFU/g vs. 3.3±4.3 x 10^5 PFU/g at 6 d.p.i.) (Fig. 3-A, B). Thus, the amelioration of disease outcome is not associated with reduced viral replication nor faster clearance. We then interrogated if the difference observed between WT and *Daf*$^{-/-}$ mice could be explained by a spatial difference in lung tissue infection, as was previously described for milder disease progression (45). To detect infected cells in specific parts of the lung tissue, we performed immunohistochemistry (IHC) staining of viral nucleoprotein (NP) in mice lung sections at 3 d.p.i., time corresponding to higher viral loads. A blind qualitative observation elucidated that in both WT and *Daf*$^{-/-}$ mice, infection foci were mainly restricted to alveoli (Fig. 3-C), and quantification of infected bronchioli per lung section did not display relevant dissimilarities (27.8±12.7 in WT and 28.4±9.8 in *Daf*$^{-/-}$) (Fig. 3-D).

Lastly, to assess if protection of *Daf*$^{-/-}$ mice was linked to a decrease in lung damage and immunopathology, a comprehensive and blind histological analysis of lung tissue was performed at day 3 and 6 p.i. (Table S1). At 3 d.p.i., *Daf*$^{-/-}$ mice had a histological score of 4.0±1.3, whereas WT mice had a score of 5.4±2.0 (Fig. 3-E). At 6 d.p.i., this difference became significant, with *Daf*$^{-/-}$ mice having a score of 10.8±2.2, and WT of 12.8±2.6 (Fig. 3-F). Therefore, IAV infected *Daf*$^{-/-}$ mice have reduced lung damage at 6 d.p.i., when

compared to their WT counterparts, demonstrating that DAF increases tissue damage. These results show that DAF does not impact viral replication, clearance nor spatial distribution in the lungs, but point to a new role for DAF as an immunopathology instigator.

DAF-induced immunopathology relies on elevated complement activation, immune cell recruitment and levels of IFN-γ.

We have shown that *Daf*$^{-/-}$ mice suffer less severe disease than WT mice upon IAV infection by decreasing tissue damage. Next, we aimed at dissecting the mechanism. DAF being an RCA, we first focused on determining the role of the complement pathway. For that purpose, C57BL/6J *C3*$^{-/-}$ (*C3*$^{-/-}$) and C57BL/6J *C3*$^{-/-}$ / *Daf*$^{-/-}$ (*C3*$^{-/-}$ / *Daf*$^{-/-}$) mice were infected with 500 PFU of PR8-HK4,6 and bodyweight loss monitored over the course of infection. As expected (46,47), *C3*$^{-/-}$ mice lost significantly more bodyweight than the WT, losing up to 20.8% of the initial bodyweight, when WT mice lost only 9.8%. *C3*$^{-/-}$ / *Daf*$^{-/-}$ mice, however, had a bodyweight loss comparable with *C3*$^{-/-}$ mice, losing up to 20.5% of the initial bodyweight (Fig. 4-A). These results show that the protection of *Daf*$^{-/-}$ mice is C3-dependent, and thus complement mediated.

DAF regulates complement activation by accelerating the decay of C3 convertases, reducing the levels of C3a. Hence, we proceeded by analyzing the levels of C3a in the bronchoalveolar lavages (BALs) of PR8-HK4,6 infected WT or *Daf*$^{-/-}$ mice. The main differences in tissue damage occurred at 6 d.p.i., and therefore we limited our analysis to that time point. Quite surprisingly, in PR8-HK4,6 infected *Daf*$^{-/-}$ mice the levels of C3a were of 439.8±474.6 ng/ml, and in WT mice of 1425.0±899.5 ng/ml (Fig. 4-B). Thus, IAV infection induced lower complement activation in *Daf*$^{-/-}$ mice than in WT mice, indicating that complement activation may play a role in increased tissue damage of WT mice. Taken together these results highlight the equilibrium needed to clear the disease without causing damage and the important role of complement in both these processes.

The complement pathway is a cascade of reactions that will release cytokines for recruitment and activation of the immune system, and culminating in the formation of a cytolytic pore (C5b-9). Our results showed that knocking out *Cd59*, inhibitor of C5b-9, does not impact disease outcome in the context of IAV infection (Fig. 2-E, F), suggesting that the protection observed in *Daf*$^{-/-}$ mice does not rely on complement-dependent cytotoxicity (CDC). To confirm this hypothesis, WT and *Daf*$^{-/-}$ murine primary lung cells were infected with PR8-HK4,6, treated with serum collected from naïve WT mice, and cell viability assessed as a measurement of CDC. *Daf*$^{-/-}$-derived lung cells were more prone to CDC than WT-derived ones, both at steady state (57.7±2.1% vs. 25.4±1.5%) and upon PR8-HK4,6 infection (72.6±2.3% vs. 38.5±5.1%). This effect is specific of complement attack, as heat-inactivated serum did not increase cell death (Fig. 4-C), and confirms that *Daf*$^{-/-}$ mice protection is not dependent on complement cytolytic attack.

Given that *Daf*$^{-/-}$ mice have lower complement activation but that protection does not depend on CDC, it should rely on the release of anaphylatoxins leading to an alteration of immune cell recruitment and/or activation. To assess this, WT and *Daf*$^{-/-}$ mice were infected with 1000 PFU of PR8-HK4,6 and the recruitment of specific immune cell types measured in BALs. Analyses were carried at 3 and 6 d.p.i. in order to uncouple the first rapid response from a more mature later one. At 3 d.p.i. we observed that *Daf*$^{-/-}$ mice had similar numbers of natural killer (NK) cells and neutrophils recruited to the lungs, when compared to WT mice (84.4±16.8% vs. 100±71.0% NK cells; 79.7±47.4% vs. 100±59.3% neutrophils), but lower numbers of monocytes (66.3±30.3% vs. 100±25.6%) (Fig. 4-D-F). At 6 d.p.i., *Daf*$^{-/-}$ mice maintained the lower number of monocytes when compared to WT mice (58.1±30.3% vs. 100±35.8%), and also had reduced levels of neutrophils (69.1±28.8% vs. 100±27.5%) (Fig. 4-G, H). Levels of NK cells were not analyzed at this time point, nor in following analysis, as depletion of NK cells in PR8-HK4,6 infected WT mice did not alter disease outcome (Fig. S1-A, B). Additionally, we analyzed recruitment of

adaptive immune cells, namely $CD4^+$ and $CD8^+$ T cells that have been shown to play an important role in IAV infection (48). Interestingly, there was no difference in recruitment of both $CD4^+$ and $CD8^+$ T cells (Fig. 4-I, J), indicating that the protection observed in *Daf*$^{-/-}$ mice is likely dependent on lower immunopathology mediated by the innate immune response.

Cytokines are also key players in the recruitment and activation of the immune system. IFN-γ, in particular, is an essential player in viral responses, and, like all members of the immune system, can cause tissue damage. Indeed, it has recently been shown that IFN-γ, which is produced upon IAV infection, is detrimental to the host by suppressing the protective effect of group II innate lymphoid cells (ILC2) (49). Therefore, levels of IFN-γ were measured in BALs of PR8-HK4,6-infected WT and *Daf*$^{-/-}$ mice at 6 d.p.i.. *Daf*$^{-/-}$ mice had significantly lower levels of IFN-γ than WT (22.9±24.3 pg/mL vs. 44.4±32.5 pg/mL) (Fig. 4-K), which is in accordance with the reduced IL6, immunopathology and tissue damage in this context.

Taken together, these results suggest that lower complement activation leads to a reduced immune response and recruitment of innate immune cells, such as neutrophils and monocytes. This will allow a reduction in tissue damage, ameliorating disease outcome. Interestingly, and counter-intuitively, the decrease in complement activation is a consequence of the absence of a major complement regulator, DAF.

DAF-induced immunopathology depends on viral HA and NA.

We observed that lack of DAF protected mice from infection with PR8-HK4,6, but not with PR8 (Fig. 2-A-D). These strains differ only in haemagglutinin (HA) and neuraminidase (NA) (44). To investigate the individual role of these proteins in the resilience to infection, we constructed chimeric viruses in PR8 background containing either HA (PR8-HK4) or NA (PR8-HK6) from HK68. It is important to note that analyses

are performed in comparison with PR8-HK4,6 infections and not PR8. Therefore, it is the removal of HK6 in PR8-HK4 that will allow investigating the contributions of different NAs, and the removal of HK4 in PR8-HK6 that will enable assessment of the contributions of HAs.

On a first step, *Daf*$^{-/-}$ and WT mice were infected with PR8-HK6, hence highlighting the role of HA. Infection with a sublethal dose of PR8-HK6 resulted in a modest amelioration of bodyweight loss in *Daf*$^{-/-}$ mice, reaching -16.8% of the initial bodyweight, when compared to WT mice that lost up to 20.1% of the initial bodyweight (Fig. 5-A). When infected with lethal doses of this strain, both *Daf*$^{-/-}$ and WT mice had a mortality of 100% (Fig. 5-B). *In vitro* and *ex vivo* experiments had shown that this strain had increased replication levels when compared to PR8, PR8-HK4,6 or PR8-HK4 (Fig. S2-A-E). Therefore, we hypothesized that the increased mortality of *Daf*$^{-/-}$ mice, when compared to infection with the other strains, could be due to increased viral titers. Interestingly, analysis of lung viral loads showed no difference between *Daf*$^{-/-}$ and WT mice both at 3 and 6 d.p.i. (Fig. 5-C, D) and titers were not higher that those observed for the infection with PR8-HK4,6 (Fig. 3-A, B). Therefore, HA-DAF interaction modulates virulence, without impacting in viral replication or clearance *in vivo*.

As HA is involved in adhesion of viral particles to host cells, we asked if differences in HA would impact tissue penetration. As observed in PR8-HK4,6 infected mice, IHC of NP and quantification of infected bronchioli showed no difference in infection levels and patterns between *Daf*$^{-/-}$ and WT mice (Fig. 5-E, F), indicating that HA-DAF interaction has no role in this context. Additionally, analysis of tissue damage showed that histological scores between *Daf*$^{-/-}$ and WT mice were similar at 3 d.p.i. (4.7±3.5 vs. 4.1±2.8) (Fig. 5-G), but significantly reduced in *Daf*$^{-/-}$ mice when compared to WT at 6 d.p.i. (7.4±3.7 vs. 10.9±2.8) (Fig. 5-H). These results show that HA-DAF interaction contributes to disease severity and worse disease outcome observed in WT mice, but does not impact lung

306 tissue damage and hence does not completely explain the protective effect of DAF
307 absence.

308 To better understand the role of HA-DAF interaction in disease outcome, we
309 analyzed complement and immune cell recruitment in the lungs of PR8-HK6 infected mice.
310 Interestingly *C3*$^{-/-}$ and *C3*$^{-/-}$ / *Daf*$^{-/-}$ mice had similar bodyweight loss when infected with
311 PR8-HK6 (Fig. 6-A), and the levels of C3a were reduced in BALs of *Daf*$^{-/-}$ mice when
312 compared to their WT counterparts (178.4±36.8ng/mL vs. 405.8±99.2ng/mL) (Fig. 6-B).
313 These observations correspond to what was seen in PR8-HK4,6 infection and indicate that
314 different HA-DAF interactions do not elicit different complement responses.

315 Analysis of lung immune cell recruitment in PR8-HK6 infected mice showed that at 3
316 d.p.i. levels of neutrophils and monocytes were identical between *Daf*$^{-/-}$ and WT mice (Fig.
317 6-C, D). At 6 d.p.i, however, *Daf*$^{-/-}$ mice had lower numbers of neutrophils and monocytes
318 when compared to their WT counterparts (58.6±21.3% vs. 100±36.41% neutrophils;
319 61.4±19.6% vs. 100±41.45% monocytes) (Fig. 6-E, F) showing that a change in HA does
320 not alter the innate immune cell recruitment observed in PR8-HK4,6. Of note, the levels of
321 $CD4^+$ and $CD8^+$ T cells were decreased in PR8-HK6 infected *Daf*$^{-/-}$ mice when compared
322 to their WT counterparts (57.5±26.2% vs. 100±35.9% $CD4^+$ T cells and 49.3±36.7% vs.
323 100±50.5% $CD8^+$ T cells) (Fig. 6-G, H), contrarily to what was seen in PR8-HK4,6 infection
324 (Fig. 4-I, J) and showing that HA-DAF interaction modulates the adaptive immune
325 response.

326 Taken together, our data is consistent with the HA-DAF interaction controlling
327 disease severity, without impacting complement or innate immune responses leading to
328 immunopathology. It does, however, impact the recruitment of T cells. The decreased
329 activation of the adaptive immune response, together with the higher virulence of this
330 strain may exceed the beneficial effect of reduced tissue damage and explain the similar
331 mortality in *Daf*$^{-/-}$ and WT mice.

As HA-DAF interaction did not impact complement nor innate immune responses, we proceeded with analysis of NA-DAF interactions. Following the principle stated above, analyses were done in comparison with PR8-HK4,6 and not PR8 and thus the removal of HK6 from PR8-HK4,6 allowed assessing the role of different NAs. Therefore, to understand the contribution of NA in the protection conferred by DAF depletion, *Daf*$^{-/-}$ and WT mice were infected with sublethal and lethal doses of PR8-HK4. Upon infection with this strain, *Daf*$^{-/-}$ mice showed a reduced bodyweight loss when compared to the WT mice (17.7% vs. 21.8% maximum bodyweight loss) (Fig. 7-A). The detrimental effect of DAF was more evident when mice were challenged with lethal doses. Indeed, 87.5% of WT mice succumbed to infection with 250 PFU of PR8-HK4, whereas all of *Daf*$^{-/-}$ mice survived (Fig. 7-B). As these results correspond to what was observed with PR8-HK4,6, NA-DAF interaction does not directly impact disease severity.

Similarly, lung viral loads were identical in *Daf*$^{-/-}$ and WT mice infected with PR8-HK4 both at 3 (2.2±1.9 x 10^6 PFU/g vs. 4.1±5.5 x 10^6 PFU/g) and 6 d.p.i. (8.8±9.9 PFU/g x 10^4 vs. 6.1±4.1 x 10^4 PFU/g). Also, PR8-HK4 infection foci were mainly restricted to the alveoli with no difference at the level of infected bronchioli in *Daf*$^{-/-}$ and WT mice lung sections (25.8±8.3% vs. 24.2±13.6%) (Fig. 7-E, F). These results show that NA-DAF interaction does not impact viral replication, clearance or tissue penetration. Interestingly, further analysis of PR8-HK4 infected lungs showed that the lungs of *Daf*$^{-/-}$ mice were more damaged at 3 d.p.i. with a histological score of 4.3±0.9, when compared to lungs from WT mice that had a score of 2.9±1.5. At 6 d.p.i. this difference was no longer present, *Daf*$^{-/-}$ lungs having a score of 8.3±3.8, and WT of 9.2±3.1. Hence PR8-HK4 infected *Daf*$^{-/-}$ mice have more lung tissue damage at an early time point in infection, when compared to WT mice, and oppositely to what was observed in PR8-HK4,6 infection. NA-DAF interaction would then control lung immunopathology in this context, but with no real consequence in

357 disease outcome, as *Daf*$^{-/-}$ still had decreased bodyweight loss and mortality when
358 compared to the WT.

359 To better understand the mechanism behind this observation, we started by
360 assessing the role of complement. *C3*$^{-/-}$ / *Daf*$^{-/-}$ and *C3*$^{-/-}$ mice had a similar bodyweight loss
361 upon PR8-HK4 infection (Fig. 8-A), and *Daf*$^{-/-}$ mice had significantly lower levels of C3a
362 detected in BALs at 6 d.p.i. when compared to their WT counterparts (194.4±115.6 ng/mL
363 vs. 506.4±180.2 ng/mL) (Fig. 8-B). These results confirm that, similarly to what was
364 observed in PR8-HK4,6 and PR8-HK6 infections, the protection of *Daf*$^{-/-}$ mice upon PR8-
365 HK4 infection is complement mediated, and *Daf*$^{-/-}$ mice might be protected via lower levels
366 of complement activation.

367 We then proceeded with analysis of immune cell recruitment to the lungs at 3 and 6
368 d.p.i.. At 3 d.p.i., *Daf*$^{-/-}$ mice had reduced levels of neutrophils but not monocytes when
369 compared to their WT counterparts (16.2±8.6% vs. 100±112.1% neutrophils; 38.1±21.1%
370 vs. 100±79.5% monocytes) (Fig. 8-C, D). Then, at 6 d.p.i., *Daf*$^{-/-}$ and WT mice had
371 comparable levels of both neutrophils and monocytes, and $CD4^+$ and $CD8^+$ T cells (Fig. 8-
372 E-J) (105.0±62.9% vs. 100±49.2% neutrophils; 104.5±54.0% vs. 100±49.1% monocytes;
373 106±67.0% vs. 100±61.7% $CD4^+$ T cells; 104.3±60.6% vs. 100±52.6% $CD8^+$ T cells).
374 These results do not correspond to what was observed in infections with PR8-HK4,6,
375 where the main differences between *Daf*$^{-/-}$ and WT mice resided in reduced numbers of
376 monocytes at 3 d.p.i., and reduced numbers of both neutrophils and monocytes at 6 d.p.i.
377 (Fig. 4-E-H). We can therefore conclude that different NA elicit different innate immune
378 responses, and that NA-DAF interaction is responsible for the recruitment of innate
379 immune cells.

380 In summary, *Daf*$^{-/-}$ mice are protected from PR8-HK4 infection with decreased
381 complement levels and reduced neutrophil recruitment but increased immunopathology
382 early in infection. At later time points we did not observe differences between WT and *Daf*

383 $^{/-}$ mice regarding both lung tissue damage and immune cell recruitment. The reduction in
384 neutrophil recruitment reflects what was observed in PR8-HK4,6 infection, albeit at an
385 earlier time point. One might then suggest that NA-DAF interaction is important in
386 regulation of neutrophil recruitment, and that these cells play an important role in
387 modulating disease outcome. Taken together, our results demonstrate that both HA and
388 NA play a role in disease severity, and that the cumulative effect of both HA- and NA-DAF
389 interactions results in the mechanism worsening the outcome observed upon Cal, Eng and
390 PR8-HK4,6 infections.
391
392 **Influenza A virus NA cleaves DAF through its sialidase activity**
393 NA is an widely studied sialidase with described roles in mucus penetration, cell egress
394 and recently even in viral entry (50). Remarkably, NA has also been reported to cleave
395 sialic acid residues from exogenous proteins inside the cell (51). As DAF is a highly
396 sialylated protein, we hypothesized that the interaction between DAF and NA resided in
397 the ability of NA to cleave DAF's sialic acid content. Sialic acids that reside on cell surface
398 glycoproteins and glycolipids are the receptors for IAV, recognized by HA for viral entry
399 and cleaved by NA for viral exit (52). In order to assess cleavage of DAF's sialic acid
400 content, we infected a human alveolar cell line (A549) with Cal, Eng, PR8 and PR8-HK4,6,
401 and analyzed DAF content by western blot. We observed that in infected cells the band
402 marked by the anti-DAF antibody was at a lower molecular weight (MW) than in mock-
403 infected cells (Fig. 9-A). This difference in MW is of nearly 18 kDa, which corresponds to
404 DAF sialic acid content (53) and suggests that infection leads to loss of said content.
405 Quantification of this cleavage confirmed that it is dependent on infection and progressive
406 over time. Interestingly, the extent of DAF cleavage is not identical in cells infected with
407 different IAV strains, PR8 infected cells presenting the most drastic effect (Fig. 9-B).

Protein glycosylation type and levels may greatly vary between organisms (54). As previous results were obtained using human cell lines, we wanted to confirm that infection with the tested strains would remove the sialic acid content of murine DAF. For that purpose, we collected mouse embryonic fibroblasts (MEF) from WT mice and infected them with the laboratory adapted strains PR8 and PR8-HK4,6. Similarly to what was shown in a human cell line infection, murine DAF in infected MEFs suffered a drop in MW, when compared to non-infected cells (Fig. 9-C). Moreover, the differences in cleavage efficacy between PR8 and PR8-HK4,6 were maintained (Fig. 9-D), showing that IAV is able to process murine DAF and giving an insight to what may be triggering complement activation *in vivo*.

To show that NA mediates processing of DAF and discard the involvement of other viral proteins, we transfected HEK293T cells with eight different plasmids, each encoding a different PR8 genomic segment. As expected, cleavage only occurred when cells were transfected with segment 6, which encodes for NA, showing that NA is the only viral protein responsible for the reduction in DAF MW (Fig. 9-E). To confirm that this drop in MW was indeed the result of direct enzymatic activity of NA, we introduced the mutation E229A in PR8 segment 6, which pronouncedly decreases NA enzymatic activity, while still sustaining a low level of viral replication (55). Using the RG technique as mentioned above, we created a PR8 strain containing the mutated NA: PR8 NA-E229A. Analysis of DAF in cells transfected with the eight RG plasmids required for producing the passage 0 virus showed that, by impairing NA sialidase activity, DAF cleavage was prevented (Fig. 9-H). Taken together, these results confirm that DAF cleavage observed upon infection is due solely to NA sialidase activity.

As NA is a transmembrane protein with potential to cleave sialic acids at the cell surface, but also in the cytoplasm while en route to the plasma membrane, we questioned where DAF cleavage was taking place. For that, PR8 infected A549 cells were treated with a non-

434 permeable NA inhibitor, Zanamivir. We observed that Zanamivir treatment reduced the
435 proportion of cleaved DAF (0.60 vs. 0.75), showing that DAF cleavage happens in part at
436 the cell membrane, and in part in the cytoplasm (Fig. 9-F, G).
437 NA unprecedented direct and pronounced effect on DAF strongly suggests a functional
438 consequence. It has been proposed that DAF negatively charged sialic acids function as a
439 spacer, which projects DAF RCA domains to the extracellular milieu (56). Additionally,
440 sialic acid removal promotes DAF to be proteolytically shed (35). Therefore, we
441 hypothesized that NA-mediated sialic acid cleavage would result in DAF loss/alteration of
442 function, resulting in increased complement activity. To test this, we produced lentiviral
443 vectors to deliver WT or E229A versions of PR8 NA fused to GFP. After transduction of
444 A549 cells, we treated cells with normal human serum and stained for C5b-9 as a proxy for
445 complement activation. Transduction of cells with WT NA resulted in increased C5b-9
446 deposition when compared with cells transduced with E229A (1±0.7 vs. 0.3±0.2) (Fig. 9-I).
447 Therefore, NA removal of DAF sialic acid content does impair its complement regulator
448 function, increasing complement activation.
449 For IAV receptor recognition, the binding of sialic acid to the penultimate galactose
450 residues of carbohydrate side chains is important, and different IAVs exhibit preference for
451 Neu5Ac α(2,3)-Gal (hereafter α2,3-) or Neu5Ac α(2,6)-Gal (hereafter α2,6-) conformations
452 (57,58). Interestingly, most avian IAVs bind preferentially to sialic acid joined to the sugar
453 chain through an α2,3-linkage, whereas human IAV preferentially use α2,6-linked sialic
454 acid as a cellular receptor (58,59). To assess which type of ligations were cleaved by NA,
455 we infected A549 cells with PR8 and purified DAF by immunoprecipitation. Subsequently,
456 we treated immunoprecipitated DAF with PNGaseF to remove N-glycans, and probed DAF
457 by western blot and lectin blot with *Sambucus nigra* agglutinin (SNA), which detects α2,6-
458 linked sialic acid (Fig. 9-J). The cumulative effect in DAF MW decrease of PR8 infection

and PNGaseF treatment, as well as loss of SNA staining only upon infection, indicates that PR8 infection specifically removes α2,6-linked sialic acid from DAF O-glycans.

The affinity of the IAV HA and NA for respective sialic acid conformation is one of the host species restriction factors (60), avian strains preferring α2,3-linked sialic acids, whereas human strains are able to cleave α2,6-linked sialic acids. In accordance with that, transfection of HEK293T cells with avian-adapted NAs did not impact DAF MW (Fig. 9-K). Remarkably, transfection with NAs from a H7N9 isolated from a human patient (A/Anhui/1/2013) and from a H5N6 isolated from a chicken (A/chicken/Jiangxi/02.05 YGYXG023-P/2015) caused a drop in DAF MW. These two NAs are thus able cleave α2,6-linked sialic acid residues, indicating they are already adapted to human sialic acid linkages and indeed both H7N9 (61,62) and H5N6 (63,64) strains have been shown to cause severe zoonotic disease. These results suggest that analysis of sialic acid cleavage might be worth exploring as a measure for host adaptation and zoonotic events.

Overall, our results unveil DAF as a novel host virulence factor upon IAV infection, depending on interaction with HA and NA. Specifically, we observed a widespread direct interaction between NA and DAF with functional implications, which is an unprecedented way of a virus, via altering a host protein from within the infected cell, modulating the immune response.

Discussion

This work highlights the importance of a balanced immune response to viral infections in order to clear the disease without causing immunopathology. Despite its intrinsic protective role, complement is a documented driver of immunopathology in severe viral infections such as IAV (31–33), SARS-CoV-2 (28–30) and MERS (27). In the context of IAV, inhibition of different components of the complement system such as C3a receptor and C5 decreased immune cell recruitment and activation leading to an ameliorated disease outcome (31–33). Our work is in accordance with these studies as *Daf*$^{-/-}$ mice have less severe disease upon IAV infection, coupled with reduced C3a levels in BALs, and a lower number of immune cells recruited to the lungs (Fig. 4-A, B, 6-A, B, 8-A, B). However, C3 is essential in IAV infection. *C3*$^{-/-}$ and *C3*$^{-/-}$ / *Daf*$^{-/-}$ mice had increased mortality when compared to the WT (Fig. 3-A; 6-A; 8-A) and *C3*$^{-/-}$ mice presented increased lung inflammation and infiltration of immune cells upon IAV infection (47,65). These observations show the potential of regulating complement activation as a strategy to provide resilience to viral infections, without affecting pathogen clearance.

Interestingly, infection of *Cd59*$^{-/-}$ mice and analysis of CDC in WT and *Daf*$^{-/-}$ primary lung cells indicated that the last step of the complement cascade does not impact disease outcome in IAV infection (Fig. 2-E, F; 4-C; S2-F, G). Rather, it suggests that earlier components of the complement cascade, such as anaphylatoxins C3a and/or C5a have a modulatory role of IAV virulence. This hypothesis agrees with the function of C3a and C5a as recruiters and activators of the innate immune response, which can lead to immunopathology (31–33). Our results indicate that, in fact, and contrary to expected, in IAV infection, lack of DAF leads to reduced activation of complement, lower levels of C3a and decreased recruitment of monocytes and neutrophils, specifically. The lower levels of C3a detected in the BALs of *Daf*$^{-/-}$ mice could explain the lower numbers of innate immune

cells recruited, and decreased tissue damage. However, compared to PR8-HK4,6, infection with PR8-HK6 altered recruitment of adaptive immune cells, and PR8-HK4 of innate immune cells, without changing the levels of C3a in *Daf*$^{-/-}$ mice. These results indicate that complement is not the sole recruiter and activator of the immune response, and that a direct or indirect HA-DAF and/or NA-DAF interaction has additional roles to play in immune cell recruitment.

In fact, we found that HA-DAF interplay impacts recruitment of $CD4^+$ and $CD8^+$ T cells, both of which shown to be essential in the clearance of IAV (66). The lower levels of these cells in *Daf*$^{-/-}$ mice might annul the beneficial effect of lower lung tissue damage observed at 6 d.p.i.. Indeed, upon PR8-HK6 challenge, mice bodyweight rapidly dropped at 7 d.p.i., whereas in infection with other viral strains loss of weight started around 4 d.p.i. and was more gradual, suggesting that the adaptive immune system is implicated in the process (9,67). Despite HA being amongst the most immunogenic proteins of IAV, and hence its involvement in adaptive immune response not surprising (67,68), our work shows for the first time a specific interaction of HA with DAF and the implications of this axis in T cell recruitment.

We also identified a novel function for the viral protein NA, via cleaving sialic acids of DAF and modulating immune cell recruitment and viral pathogenicity. Remarkably, NA-mediated cleavage of another host protein, latent TGF-β, activates it, which confers a protective role upon infection (69,70). Here we found that NA cleaves α2,6-linked sialic acids from DAF and hypothesize that this could explain the differences in the numbers of neutrophils and monocytes recruited to the site of infection. Ablation of neutrophils in IAV infections have been shown to prevent tissue damage without affecting viral loads (71–74). In fact, these cells have long been associated with acute respiratory distress syndrome (75), and extensive neutrophil infiltration and release of neutrophil extracellular traps (NETs) have been linked to increased pneumonia severity in critical cases of COVID-19

(76–78). Despite these observations, neutrophils are important to the host response against IAV infection as neutrophil depletion resulted in exacerbated viral loads, lung damage and mortality in mice infected with PR8-HK4,6 (79,80). In addition to neutrophils, monocytes are readily recruited to sites of IAV challenge where they differentiate into macrophages or dendritic cells (DC) (81,82) that share many properties with their conventional counterparts (83) and have been studied upon IAV infection (83,84). Monocyte-derived macrophages contribute to the inflammation resolution by clearing apoptotic neutrophils and confer lasting protection against secondary bacterial infections (84,85). The interaction with apoptotic neutrophils has also been reported to increase differentiation of monocytes into DC, promoting adherence of $CD8^+$ T cells (85). Conversely, monocyte and monocyte-derived cells may contribute to immunopathology, as their depletion decreased disease severity without altering viral loads (86–88). These studies show that both cell types are essential for IAV infection but can contribute to tissue damage, and support our hypothesis that increased immunopathology of WT mice upon IAV infection is mediated by excessive recruitment of neutrophils and monocytes.

The link we identified via NA, DAF and complement establishes a viral mediated mechanism for maintaining inflammation via increasing the recruitment of immune cells. The model that we propose and that is depicted in Figure 10 explores an interplay between HA and NA in modulating the immune response. Previous examples include the activation of the NK cell sialylated receptors NKp44 and NKp46 by HA at the surface of infected cells, which is countered by NA-mediated desialylation (89,90). In the case of our work, it is known that apical delivery of NA to the cell surface is potentiated by HA (91) and during this transport (and also at the plasma membrane), NA would cleave DAF sialic acid giving rise to increased activation of complement. Indeed, we observed that IAV infection induces a drop in DAF MW over the course of infection both in human and murine cell lines. The drop corresponds to DAF sialic acid content, and NA is necessary and sufficient

556 for this cleavage (Fig. 9-A, C, E, H and J). Moreover, transduction of cells with NA and
557 thus removal of DAF sialic acid content resulted in an increased C5b-9 deposition (Fig. 9-
558 I). We propose that the removal of DAF sialic acid content would not lead to a loss of
559 function, but instead trigger an exaggerated complement response. This is contrary to
560 what is observed for autoimmune diseases, for which *Daf*$^{-/-}$ mice have been widely used
561 (92–94). These mice have increased disease severity coupled with high complement
562 activation levels when compared to their WT counterparts, showing that *Daf*$^{-/-}$ mice do not
563 lack the ability to activate the complement and that the mechanism we now describe could
564 be shared among viruses containing promiscuous NAs. As an alternative, NA-mediated
565 DAF cleavage could result in the recruitment of innate immune cells by exposing “non-self”
566 glycans at cell surface, which has been shown to activate complement via the lectin
567 pathway (95). Besides complement, it could also be recognized by different PRRs (96). At
568 the moment this hypothesis is speculative but raises concerns about using therapies, such
569 as DAS181 (97), aiming at decreasing sialic acid levels at cell surface to prevent viral
570 entry. Interestingly, our work indicates that NA cleavage of sialic acids does not happen
571 solely at the cell surface, but also in the cytoplasm, as treatment with Zanamivir did not
572 completely abolish DAF cleavage (Fig. 9-F). To the best of our knowledge, this mechanism
573 has not been reported before.

574 DAF cleavage provides a possible link between DAF-NA interaction and *in vivo*
575 pathology. Given that our study shows that sialic acids cleaved by DAF are α2,6-linked to
576 O-glycans, this mechanism may have implications in host species jumps, as for example,
577 IAV adapted to birds exhibit preference for α2,3-linked sialic acids. Interestingly, we
578 present evidence that NAs derived from two avian-adapted strains, H5N6 and H7N9, were
579 able to cleave human DAF (Fig. 9-J). As H7N9 and H5N6 outbreaks provoked severe
580 infections in humans, associated with exacerbated immune response (61–63),

hypothetically establishing DAF cleavage as a hallmark of virulence could be a useful tool to monitor viruses with pandemic potential.

In addition, many host proteins including mucins are decorated by sialic acids. Mucins form an important barrier at the cell surface preventing viral entry (98). These proteins are also heavily glycosylated, specifically at the terminal part of O-glycans (99), similarly to DAF, indicating that they could be substrates of NA. As a consequence, the mechanism we describe could be used to manipulate the extracellular environment and facilitate viral cell-to-cell transmission. Identification of glycans exposed at the surface of infected cells and their interaction with viral proteins may help understand the balance between viral entry and immune response targets and reveal disease resilience pathways prone to therapeutic intervention.

Materials & methods

Statistical analyses

All statistical analyses were conducted using GraphPad Prism 6. Detailed statistics and number of replicates for all experiments can be found in the figure legends and/or in the manuscript. Bodyweight loss and DAF cleavage: Statistical significance represented as *p < 0.05, **p < 0.01, ***p < 0.001, using two-way ANOVA followed by Holm-Sidak multiple comparisons test. Survival curves: Statistical significance compared with WT using Log-rank (Mantel-Cox) test. Compare two groups: Population normality assessed with D'Agostino & Pearson omnibus normality test. Statistical significance using unpaired t-test with Welch's correction for normal populations or Mann-Whitney test for populations whose normality was not proved; Wilcoxon matched-pairs signed rank test for populations whose normality was not proved, but samples were paired. Multiple comparisons: Population normality assessed with D'Agostino & Pearson omnibus normality test. Kruskal-Wallis followed by Dunn's multiple comparisons test for populations whose normality was not proved.

Ethics statement

All experiments involving mice were performed using 8-week-old littermate C57BL6/6J, C57BL6/6J *Daf*$^{-/-}$, C57BL6/6J *Cd59*$^{-/-}$, C57BL6/6J *C3*$^{-/-}$ or C57BL6/6J *C3*$^{-/-}$ / *Daf*$^{-/-}$ female mice under specific pathogen-free conditions at the Instituto Gulbenkian de Ciência (IGC) biosafety level 2 (BSL-2) animal facility. Animals were group housed in individually ventilated cages with access to food and water *ad libitum*. This research project was ethically reviewed and approved by both the Ethics Committee and the Animal Welfare Body of the IGC (license references: A016/2013 and A013/2019), and by the Portuguese National Entity that regulates the use of laboratory animals (DGAV – Direção

619 Geral de Alimentação e Veterinária (license references: 0421/000/000/2015 and
620 0421/000/000/2020). All experiments conducted on animals followed the Portuguese
621 (Decreto-Lei nº 113/2013) and European (Directive 2010/63/EU) legislations, concerning
622 housing, husbandry and animal welfare.
623
624 Mice infection, lung, BAL and tissue analysis.
625 All mice experiments were conducted in a BSL-2 animal facility. Littermates were
626 randomly allocated to experimental conditions. Mice were anesthetized with isoflurane
627 (Abbot) and 30µL of inoculum administered intranasally. Mice were daily monitored for 11
628 days or sacrificed with CO_2 at indicated timepoints. To comply with best animal welfare
629 practices, animals that lost more than 25% of their initial weight and did not recover until
630 the next day were sacrificed. Tissues were collected in aseptic conditions.
631 Lung viral loads were collected from right lower lobes using tungsten carbide beads
632 (Qiagen) in a TissueLyser II (Qiagen) at $20s^{-1}$ for 3min. After centrifugation, supernatants
633 were collected and titrated by plaque assay (100,101).
634 Bronchoalveolar lavage (BAL) of the whole lung was performed with 1ml sterile
635 PBS via tracheal cannula. After centrifugation, supernatants were used for ELISA analysis
636 (Mouse C3a (TECOmedical, TE1038) or Mouse IFN-γ DuoSet ELISA (R&D Systems,
637 DY485)), following manufacturer's instructions, and cells analyzed by flow cytometry.
638 Unspecific staining was minimized with Fc blocking (rat anti-mouse CD16/CD32, IGC
639 antibody facility, clone 2.4G2). Cells were incubated with primary antibodies (Table S2) in
640 FC buffer, 20min at 4ºC, stained with Zombie Aqua™ Fixable Viability Kit (BioLegend,
641 423101) and fixed with IC fixation buffer according to manufacturer's recommendations.
642 Flow cytometry analysis of cell populations was performed in a BD LSR Fortessa X-20
643 SORP (BD Biosciences) equipped with BD FACSDiva™ 8 and FlowJo 10 software (Tree

644 Star Inc., Ashland, OR, USA), and absolute numbers obtained with Perfect-Count
645 Microspheres™ (Cytognos, CYT-PCM).
646
647 Immune cell depletion
648 Natural killer (NK) cells were depleted by intraperitoneal (IP) injection of 200µg α-
649 NK1.1 (IGC antibody facility, clone PK136) in 200µl PBS every 72h, starting 72h before
650 infection.
651
652 Histology and immunohistochemistry (IHC)
653 Histological scoring was conducted as in (45), and expressed as the sum of the
654 parameter described in Table S1. Scoring was performed blindly by a pathologist. For IHC
655 tissue sections were deparaffinized, rehydrated, and heated in citrate buffer (40mM
656 sodium citrate dihydrate, 60mM citric acid, pH 6) and blocked with 1:50 Fc block reagent
657 (rat anti-mouse CD16/CD32, IGC antibody facility, clone 2.4G2). Slides were then
658 incubated with rabbit α-NP (102) 1:1000 for 16h at 4ºC. After blocking of endogenous
659 peroxidases sections were incubated with ImmPRESS® HRP Horse Anti-Rabbit IgG
660 Polymer Detection Kit (Vector Laboratories, MP-7401-15) for 1h at RT and then with DAB
661 substrate (Roche, 11718096001) according to manufacturer's instructions. Finally, lung
662 sections were contrasted with Mayer Hematoxylin and images taken in a NanoZoomer-SQ
663 Digital slide scanner (Hamamatsu Photonics).
664
665 Complement dependent toxicity and C5b-9 deposition
666 Lung primary cells from WT or *Daf*$^{-/-}$ mice were infected as described below with
667 indicated IAVs for 12h, collected and suspended in veronal buffer (CompTech, B100).
668 Serum from WT mice (or heat-inactivated at 56ºC, 30min) was added at a final
669 concentration of 50% (v/v) and incubated at 37ºC, 5% CO_2 for 1h. Viability was assessed

by flow cytometry using Zombie Aqua™ Fixable Viability Kit after fixation IC fixation buffer following manufacturer's indications.

C5b-9 deposition measurement was adapted from (103). Lentivirus encoding NA-GFP WT/E229A was added to A549 cells. Cells were then suspended in veronal buffer and human serum (Sigma-Aldrich, H4522) (or heat-inactivated for 30min at 56ºC), added at a final concentration of 50% (v/v). After 15min incubation, C5b-9 deposition was assessed by flow cytometry using α-C5b-9 (Abcam, ab55811, 1:100) and α-Mouse Alexa Fluor 647 (Invitrogen, A31571, 1:1000). Cells were fixed with IC Fixation Buffer according to manufacturer's indications.

Cell lines, transfections and infection

Madin-Darby Canine Kidney (MDCK), Human Embryonic Kidney 293 T (HEK293T), and human alveolar basal (A549) cells were a kind gift from Prof. Paul Digard (Roslin Institute, UK). Mouse embryonic fibroblasts (MEFs) were isolated from WT and *Daf*$^{-/-}$ mice E13.5 to E15.5 embryos as previously described (104). Primary lung cells were isolated from WT and *Daf*$^{-/-}$ mice. Briefly, 1.5ml of sterile collagenase D (0.5mg/ml in PBS, Roche, 11088858001) and 0.5ml of melted agarose (1% in PBS, Lonza, 50004) were instilled in lungs of mice after exsanguination and PBS perfusion. Whole lungs were then collected and incubated with collagenase D 40min at RT. After dissection in complete DMEM supplemented with 5U DNase I (NZYTech, MB19901), cells were collected and plated in a 6-well plate at a density of 9 x 10^5 cells/well and incubated for 48h at 37ºC, 5% CO_2. All cell lines were cultured in complete DMEM and incubated at 37ºC, 5% CO_2.

Transfection of HEK293T cells was performed using Lipofectamine 2000 (ThermoFisher, 11668027) according to manufacturer's recommendations. Plasmids encoding NA genes from following strains were kindly provided by Dr. Holly Shelton (The Pirbright Institute, UK) and were synthesized by GeneArt (Invitrogen) and cloned into a

pHW2000 vector (105): H6N1 A/chicken/Taiwan/67/2013 (GenBank accession no. KJ162862), H9N2 A/chicken/Pakistan/UDL-01/08 (106), H5N2 A/goose/Taiwan/01031/2015 (107), H5N6 A/chicken/Jiangxi/02.05 YGYXG023-P/2015 (107), H4N6 A/chicken/Hunan/S1267/2010 (GenBank accession no. KU160821), H10N8 A/chicken/Jiangxi/1204/2014 (GenBank accession no. KP285359), H5N8 A/scarlet ibis/Germany/Ar44-L01279/2015 (107), H7N9 A/Anhui/1/2013 (108).

One-step infections were carried out at a multiplicity of infection (MOI) of 3 in serum-free DMEM for 45min and then overlaid with complete DMEM and kept at 37 °C and 5% CO_2 for the duration of the experiment.

Western blot

Western blotting was performed according to standard procedures and imaged using a LI-COR Biosciences Odyssey Infrared Imaging System. Primary and secondary antibodies used are in Table S2.

Viruses and titration

Human circulating strains A/California/7/2009 (Cal, H1N1) and A/England/195/2009 (Eng, H1N1) were kindly provided by Prof. Paul Digard). Reverse-genetics derived A/Puerto Rico/8/34 (PR8) and A/X-31 (PR8-HK4,6) were used as model viruses. Reverse-genetics derived chimeric PR8 containing the segment 4 from A/Hong Kong/1/1968, seg4-HK68 (PR8-HK4), or the segment 6 (PR8-HK6) were produced as previously described (105,109,110). pDual plasmids were a kind gift from Dr. Ron Fouchier (Erasmus MC, Netherlands). PR8 NA-E229A (55) was generated by reverse genetics after site directed mutagenesis of pDual::segment6. All viruses were amplified in embryonated chicken eggs and titrated using plaque assay as previously described (100,101).

721 Lentivirus were produced in HEK293T cells transfected with the following plasmids
722 (ThermoFisher, OHS4735): 6µg pLEX-MCS-1::NA-GFP WT/E229A, 4.2µg psPAX2, 1.8µg
723 pMD2.G. 72h hours after transfection, medium containing lentivirus was collected and
724 stored at -80ºC.
725
726 Bacteria and cloning.
727 All transformations for cloning or plasmid amplification were performed in
728 *Escherichia coli* XL10 Gold (Agilent) according to manufacturer's instructions.
729 Viral RNA (vRNA) was extracted from egg-grown viral stocks using QIAamp Viral
730 RNA Mini Kit (Qiagen, 50952904) according to manufacturer's instructions. From purified
731 vRNA, NA cDNA was produced using NZY M-MulV First-Strand cDNA Synthesis Kit
732 (NZYTech, MB17302) with primer "NA_Fw_HindIII" following manufacturer's
733 recommendations. To produce pEGFP-N1::NA, NA was then amplified and cloned in
734 HindIII-KpnI restriction sites of pEGFP-N1. To generate pLEX-MCS-1::NA-GFP, NA-GFP
735 was amplified from pEGFP-N1::NA and cloned into NotI/XhoI sites of pLEX-MCS-1.
736 pDual::seg6-E229A and pEGFP-N1::NA-E229A were generated by site directed
737 mutagenesis of pDual::seg6 and pEGFP-N1::NA respectively, using the QuikChange Site-
738 Directed Mutagenesis Kit (Agilent, 200518), according to manufacturer's instructions.
739 Primer sequences are indicated in Table S3.
740
741 DAF glycosylation
742 A549 cells were infected with PR8 as described above. After 12h of infection, cells
743 were lysed with lysis buffer 17 (R&D Systems, 895943) and protein quantified using
744 bicinchoninic acid protein assay (BCA) (Pierce™, 23225). Protein G Sepharose 4 Fast
745 flow beads (GE Healthcare, GE17-0618-01) were incubated with α-DAF (Abcam,
746 ab133684) for 5h and then Protein G-DAF complexes were crosslinked using

747 bis(sulfosuccinimidyl)suberate (BS^3) (Sigma, S5799). Protein from total cell extracts (100
748 µg) were then added to the antibody Protein G complex and incubated 16h at 4 °C in a
749 rotator mixer. Washing steps were performed with PBS and samples used for downstream
750 analysis.

751 After DAF immunoprecipitation, removal of N-glycans was performed by digestion
752 with PNGaseF (New England Biolabs, P0704S), according to manufacturer's instructions.
753 For blotting experiments gels were transferred onto nitrocellulose and unspecific binding
754 blocked using 5% BSA and 2% polyvinylpyrrolidone (PVP) for blot detection with α-DAF or
755 biotinylated *Sambucus nigra* agglutinin (SNA) (Vector Laboratories B-1305-2),
756 respectively. DAF was detected with HRP-conjugated goat anti-rabbit (Jackson
757 ImmunoResearch, 111-035-144) and SNA with Vectastain Avidin/Biotin Complex (Vector
758 Laboratories, PK-4000) incubation. Detection was performed by enhanced
759 chemiluminescence (ECL) (GE Healthcare, RPN2232) and film sheet exposure.

760

761 **References**

762

763 1. Iwasaki A, Foxman EF, Molony RD. Early local immune defences in the respiratory
764 tract. Nat Rev Immunol. 2017 Jan;17(1):7–20.
765 2. Iwasaki A, Pillai PS. Innate immunity to influenza virus infection. Nat Rev Immunol.
766 2014 May;14(5):315–28.
767 3. Gargaglioni LH, Marques DA. Let's talk about sex in the context of COVID-19. J
768 Appl Physiol Bethesda Md 1985. 2020 Jun 1;128(6):1533–8.
769 4. Gebhard C, Regitz-Zagrosek V, Neuhauser HK, Morgan R, Klein SL. Impact of sex
770 and gender on COVID-19 outcomes in Europe. Biol Sex Differ. 2020 May 25;11(1):29.
771 5. Haitao T, Vermunt JV, Abeykoon J, Ghamrawi R, Gunaratne M, Jayachandran M,
772 et al. COVID-19 and Sex Differences: Mechanisms and Biomarkers. Mayo Clin Proc. 2020
773 Oct;95(10):2189–203.
774 6. Medzhitov R, Schneider DS, Soares MP. Disease tolerance as a defense strategy.
775 Science. 2012 Feb 24;335(6071):936–41.
776 7. Sell S. Immunopathology. Am J Pathol. 1978 Jan;90(1):211–80.
777 8. WHO. Influenza (Seasonal) [Internet]. [cited 2021 Feb 9]. Available from:
778 https://www.who.int/en/news-room/fact-sheets/detail/influenza-(seasonal)
779 9. Krammer F, Smith GJD, Fouchier RAM, Peiris M, Kedzierska K, Doherty PC, et al.
780 Influenza. Nat Rev Dis Primer. 2018 Jun 28;4(1):3.
781 10. Taubenberger JK, Morens DM. The pathology of influenza virus infections. Annu
782 Rev Pathol. 2008;3:499–522.
783 11. Uyeki TM. High-risk Groups for Influenza Complications. JAMA. 2020 Dec
784 8;324(22):2334.
785 12. Taubenberger JK, Morens DM. 1918 Influenza: the mother of all pandemics.
786 Emerg Infect Dis. 2006 Jan;12(1):15–22.
787 13. Melvin JA, Bomberger JM. Compromised Defenses: Exploitation of Epithelial
788 Responses During Viral-Bacterial Co-Infection of the Respiratory Tract. PLoS Pathog.
789 2016 Sep;12(9):e1005797.
790 14. Rowe HM, Meliopoulos VA, Iverson A, Bomme P, Schultz-Cherry S, Rosch JW.
791 Direct interactions with influenza promote bacterial adherence during respiratory
792 infections. Nat Microbiol. 2019 Aug;4(8):1328–36.
793 15. Siegel SJ, Roche AM, Weiser JN. Influenza promotes pneumococcal growth during
794 coinfection by providing host sialylated substrates as a nutrient source. Cell Host Microbe.
795 2014 Jul 9;16(1):55–67.
796 16. Talmi-Frank D, Altboum Z, Solomonov I, Udi Y, Jaitin DA, Klepfish M, et al.
797 Extracellular Matrix Proteolysis by MT1-MMP Contributes to Influenza-Related Tissue
798 Damage and Mortality. Cell Host Microbe. 2016 Oct 12;20(4):458–70.
799 17. Damjanovic D, Small C-L, Jeyanathan M, Jeyananthan M, McCormick S, Xing Z.
800 Immunopathology in influenza virus infection: uncoupling the friend from foe. Clin Immunol
801 Orlando Fla. 2012 Jul;144(1):57–69.
802 18. Newton AH, Cardani A, Braciale TJ. The host immune response in respiratory virus
803 infection: balancing virus clearance and immunopathology. Semin Immunopathol. 2016
804 Jul;38(4):471–82.
805 19. Arunachalam PS, Wimmers F, Mok CKP, Perera RAPM, Scott M, Hagan T, et al.
806 Systems biological assessment of immunity to mild versus severe COVID-19 infection in
807 humans. Science. 2020 Sep 4;369(6508):1210–20.
808 20. Hadjadj J, Yatim N, Barnabei L, Corneau A, Boussier J, Smith N, et al. Impaired
809 type I interferon activity and inflammatory responses in severe COVID-19 patients.
810 Science. 2020 Aug 7;369(6504):718–24.

21. Freeley S, Kemper C, Le Friec G. The “ins and outs” of complement-driven immune responses. Immunol Rev. 2016 Nov;274(1):16–32.
22. Merle NS, Church SE, Fremeaux-Bacchi V, Roumenina LT. Complement System Part I - Molecular Mechanisms of Activation and Regulation. Front Immunol. 2015;6:262.
23. Sarma JV, Ward PA. The complement system. Cell Tissue Res. 2011 Jan;343(1):227–35.
24. Radicioni G, Cao R, Carpenter J, Ford AA, Wang T, Li L, et al. The innate immune properties of airway mucosal surfaces are regulated by dynamic interactions between mucins and interacting proteins: the mucin interactome. Mucosal Immunol. 2016 Nov;9(6):1442–54.
25. Gralinski LE, Sheahan TP, Morrison TE, Menachery VD, Jensen K, Leist SR, et al. Complement Activation Contributes to Severe Acute Respiratory Syndrome Coronavirus Pathogenesis. mBio. 2018 Oct 9;9(5).
26. Wang R, Xiao H, Guo R, Li Y, Shen B. The role of C5a in acute lung injury induced by highly pathogenic viral infections. Emerg Microbes Infect. 2015 May;4(5):e28.
27. Jiang Y, Zhao G, Song N, Li P, Chen Y, Guo Y, et al. Blockade of the C5a-C5aR axis alleviates lung damage in hDPP4-transgenic mice infected with MERS-CoV. Emerg Microbes Infect. 2018 Apr 24;7(1):77.
28. Fletcher-Sandersjöö A, Bellander B-M. Is COVID-19 associated thrombosis caused by overactivation of the complement cascade? A literature review. Thromb Res. 2020 Oct;194:36–41.
29. Lo MW, Kemper C, Woodruff TM. COVID-19: Complement, Coagulation, and Collateral Damage. J Immunol Baltim Md 1950. 2020 Sep 15;205(6):1488–95.
30. Polycarpou A, Howard M, Farrar CA, Greenlaw R, Fanelli G, Wallis R, et al. Rationale for targeting complement in COVID-19. EMBO Mol Med. 2020 Aug 7;12(8):e12642.
31. Garcia CC, Weston-Davies W, Russo RC, Tavares LP, Rachid MA, Alves-Filho JC, et al. Complement C5 activation during influenza A infection in mice contributes to neutrophil recruitment and lung injury. PloS One. 2013;8(5):e64443.
32. Song N, Li P, Jiang Y, Sun H, Cui J, Zhao G, et al. C5a receptor1 inhibition alleviates influenza virus-induced acute lung injury. Int Immunopharmacol. 2018 Jun;59:12–20.
33. Sun S, Zhao G, Liu C, Wu X, Guo Y, Yu H, et al. Inhibition of complement activation alleviates acute lung injury induced by highly pathogenic avian influenza H5N1 virus infection. Am J Respir Cell Mol Biol. 2013 Aug;49(2):221–30.
34. Pandya PH, Fisher AJ, Mickler EA, Temm CJ, Lipking KP, Gracon A, et al. Hypoxia-Inducible Factor-1α Regulates CD55 in Airway Epithelium. Am J Respir Cell Mol Biol. 2016 Dec;55(6):889–98.
35. Reddy P, Caras I, Krieger M. Effects of O-linked glycosylation on the cell surface expression and stability of decay-accelerating factor, a glycophospholipid-anchored membrane protein. J Biol Chem. 1989 Oct 15;264(29):17329–36.
36. Varsano S, Frolkis I, Ophir D. Expression and distribution of cell-membrane complement regulatory glycoproteins along the human respiratory tract. Am J Respir Crit Care Med. 1995 Sep;152(3):1087–93.
37. Hoffman EM. Inhibition of complement by a substance isolated from human erythrocytes. I. Extraction from human erythrocyte stromata. Immunochemistry. 1969 May;6(3):391–403.
38. Hoffmann EM. Inhibition of complement by a substance isolated from human erythrocytes. II. Studies on the site and mechanism of action. Immunochemistry. 1969 May;6(3):405–19.
39. Kim DD, Song W-C. Membrane complement regulatory proteins. Clin Immunol

Orlando Fla. 2006 Mar;118(2–3):127–36.
40. Hillmen P, Lewis SM, Bessler M, Luzzatto L, Dacie JV. Natural history of paroxysmal nocturnal hemoglobinuria. N Engl J Med. 1995 Nov 9;333(19):1253–8.
41. Ozen A, Comrie WA, Ardy RC, Domínguez Conde C, Dalgic B, Beser ÖF, et al. CD55 Deficiency, Early-Onset Protein-Losing Enteropathy, and Thrombosis. N Engl J Med. 2017 Jul 6;377(1):52–61.
42. Lee N, Cao B, Ke C, Lu H, Hu Y, Tam CHT, et al. IFITM3, TLR3, and CD55 Gene SNPs and Cumulative Genetic Risks for Severe Outcomes in Chinese Patients With H7N9/H1N1pdm09 Influenza. J Infect Dis. 2017 Jul 1;216(1):97–104.
43. Zhou J, To KK-W, Dong H, Cheng Z-S, Lau CC-Y, Poon VKM, et al. A functional variation in CD55 increases the severity of 2009 pandemic H1N1 influenza A virus infection. J Infect Dis. 2012 Aug 15;206(4):495–503.
44. Kilbourne ED. Future influenza vaccines and the use of genetic recombinants. Bull World Health Organ. 1969;41(3):643–5.
45. Nieto A, Vasilijevic J, Santos NB, Zamarreño N, López P, Amorim MJ, et al. Mutation S110L of H1N1 Influenza Virus Hemagglutinin: A Potent Determinant of Attenuation in the Mouse Model. Front Immunol. 2019;10:132.
46. Kopf M, Abel B, Gallimore A, Carroll M, Bachmann MF. Complement component C3 promotes T-cell priming and lung migration to control acute influenza virus infection. Nat Med. 2002 Apr;8(4):373–8.
47. O'Brien KB, Morrison TE, Dundore DY, Heise MT, Schultz-Cherry S. A protective role for complement C3 protein during pandemic 2009 H1N1 and H5N1 influenza A virus infection. PloS One. 2011 Mar 9;6(3):e17377.
48. Ho AWS, Prabhu N, Betts RJ, Ge MQ, Dai X, Hutchinson PE, et al. Lung CD103+ dendritic cells efficiently transport influenza virus to the lymph node and load viral antigen onto MHC class I for presentation to CD8 T cells. J Immunol Baltim Md 1950. 2011 Dec 1;187(11):6011–21.
49. Califano D, Furuya Y, Roberts S, Avram D, McKenzie ANJ, Metzger DW. IFN-γ increases susceptibility to influenza A infection through suppression of group II innate lymphoid cells. Mucosal Immunol. 2018 Jan;11(1):209–19.
50. McAuley JL, Gilbertson BP, Trifkovic S, Brown LE, McKimm-Breschkin JL. Influenza Virus Neuraminidase Structure and Functions. Front Microbiol. 2019;10:39.
51. Fuller SD, Bravo R, Simons K. An enzymatic assay reveals that proteins destined for the apical or basolateral domains of an epithelial cell line share the same late Golgi compartments. EMBO J. 1985 Feb;4(2):297–307.
52. Hutchinson EC, Yamauchi Y. Understanding Influenza. Methods Mol Biol Clifton NJ. 2018;1836:1–21.
53. Lublin DM, Krsek-Staples J, Pangburn MK, Atkinson JP. Biosynthesis and glycosylation of the human complement regulatory protein decay-accelerating factor. J Immunol Baltim Md 1950. 1986 Sep 1;137(5):1629–35.
54. Gagneux P, Aebi M, Varki A. Evolution of Glycan Diversity. In: Varki A, Cummings RD, Esko JD, Stanley P, Hart GW, Aebi M, et al., editors. Essentials of Glycobiology [Internet]. 3rd ed. Cold Spring Harbor (NY): Cold Spring Harbor Laboratory Press; 2015 [cited 2021 Feb 9]. Available from: http://www.ncbi.nlm.nih.gov/books/NBK453067/
55. Doyle TM, Jaentschke B, Van Domselaar G, Hashem AM, Farnsworth A, Forbes NE, et al. The universal epitope of influenza A viral neuraminidase fundamentally contributes to enzyme activity and viral replication. J Biol Chem. 2013 Jun 21;288(25):18283–9.
56. Coyne KE, Hall SE, Thompson S, Arce MA, Kinoshita T, Fujita T, et al. Mapping of epitopes, glycosylation sites, and complement regulatory domains in human decay accelerating factor. J Immunol Baltim Md 1950. 1992 Nov 1;149(9):2906–13.

913 57. Bhide GP, Colley KJ. Sialylation of N-glycans: mechanism, cellular
914 compartmentalization and function. Histochem Cell Biol. 2017 Feb;147(2):149–74.
915 58. Joseph U, Su YCF, Vijaykrishna D, Smith GJD. The ecology and adaptive
916 evolution of influenza A interspecies transmission. Influenza Other Respir Viruses. 2017
917 Jan;11(1):74–84.
918 59. Rogers GN, Paulson JC. Receptor determinants of human and animal influenza
919 virus isolates: differences in receptor specificity of the H3 hemagglutinin based on species
920 of origin. Virology. 1983 Jun;127(2):361–73.
921 60. Yoon S-W, Webby RJ, Webster RG. Evolution and ecology of influenza A viruses.
922 Curr Top Microbiol Immunol. 2014;385:359–75.
923 61. Wu X, Xiao L, Li L. Research progress on human infection with avian influenza
924 H7N9. Front Med. 2020 Feb;14(1):8–20.
925 62. Zhou J, Wang D, Gao R, Zhao B, Song J, Qi X, et al. Biological features of novel
926 avian influenza A (H7N9) virus. Nature. 2013 Jul 25;499(7459):500–3.
927 63. Bi Y, Tan S, Yang Y, Wong G, Zhao M, Zhang Q, et al. Clinical and Immunological
928 Characteristics of Human Infections With H5N6 Avian Influenza Virus. Clin Infect Dis Off
929 Publ Infect Dis Soc Am. 2019 Mar 19;68(7):1100–9.
930 64. Bonilla-Aldana DK, Aguirre-Florez M, Villamizar-Peña R, Gutiérrez-Ocampo E,
931 Henao-Martínez JF, Cvetkovic-Vega A, et al. After SARS-CoV-2, will H5N6 and other
932 influenza viruses follow the pandemic path? Infez Med. 2020 Dec 1;28(4):475–85.
933 65. Kandasamy M, Ying PC, Ho AWS, Sumatoh HR, Schlitzer A, Hughes TR, et al.
934 Complement mediated signaling on pulmonary CD103(+) dendritic cells is critical for their
935 migratory function in response to influenza infection. PLoS Pathog. 2013
936 Jan;9(1):e1003115.
937 66. Topham DJ, Tripp RA, Doherty PC. CD8+ T cells clear influenza virus by perforin
938 or Fas-dependent processes. J Immunol Baltim Md 1950. 1997 Dec 1;159(11):5197–200.
939 67. Chen X, Liu S, Goraya MU, Maarouf M, Huang S, Chen J-L. Host Immune
940 Response to Influenza A Virus Infection. Front Immunol. 2018;9:320.
941 68. Krammer F. The human antibody response to influenza A virus infection and
942 vaccination. Nat Rev Immunol. 2019 Jun;19(6):383–97.
943 69. Carlson CM, Turpin EA, Moser LA, O'Brien KB, Cline TD, Jones JC, et al.
944 Transforming growth factor-β: activation by neuraminidase and role in highly pathogenic
945 H5N1 influenza pathogenesis. PLoS Pathog. 2010 Oct 7;6(10):e1001136.
946 70. Schultz-Cherry S, Hinshaw VS. Influenza virus neuraminidase activates latent
947 transforming growth factor beta. J Virol. 1996 Dec;70(12):8624–9.
948 71. Narasaraju T, Yang E, Samy RP, Ng HH, Poh WP, Liew A-A, et al. Excessive
949 neutrophils and neutrophil extracellular traps contribute to acute lung injury of influenza
950 pneumonitis. Am J Pathol. 2011 Jul;179(1):199–210.
951 72. Perrone LA, Plowden JK, García-Sastre A, Katz JM, Tumpey TM. H5N1 and 1918
952 pandemic influenza virus infection results in early and excessive infiltration of
953 macrophages and neutrophils in the lungs of mice. PLoS Pathog. 2008 Aug
954 1;4(8):e1000115.
955 73. Sakai S, Kawamata H, Mantani N, Kogure T, Shimada Y, Terasawa K, et al.
956 Therapeutic effect of anti-macrophage inflammatory protein 2 antibody on influenza virus-
957 induced pneumonia in mice. J Virol. 2000 Mar;74(5):2472–6.
958 74. Zhu B, Zhang R, Li C, Jiang L, Xiang M, Ye Z, et al. BCL6 modulates tissue
959 neutrophil survival and exacerbates pulmonary inflammation following influenza virus
960 infection. Proc Natl Acad Sci U S A. 2019 Jun 11;116(24):11888–93.
961 75. Weiland JE, Davis WB, Holter JF, Mohammed JR, Dorinsky PM, Gadek JE. Lung
962 neutrophils in the adult respiratory distress syndrome. Clinical and pathophysiologic
963 significance. Am Rev Respir Dis. 1986 Feb;133(2):218–25.

964 76. Barnes BJ, Adrover JM, Baxter-Stoltzfus A, Borczuk A, Cools-Lartigue J, Crawford
965 JM, et al. Targeting potential drivers of COVID-19: Neutrophil extracellular traps. J Exp
966 Med. 2020 Jun 1;217(6).
967 77. Java A, Apicelli AJ, Liszewski MK, Coler-Reilly A, Atkinson JP, Kim AH, et al. The
968 complement system in COVID-19: friend and foe? JCI Insight. 2020 Aug 6;5(15).
969 78. Zuo Y, Yalavarthi S, Shi H, Gockman K, Zuo M, Madison JA, et al. Neutrophil
970 extracellular traps in COVID-19. JCI Insight. 2020 Jun 4;5(11).
971 79. Tate MD, Ioannidis LJ, Croker B, Brown LE, Brooks AG, Reading PC. The role of
972 neutrophils during mild and severe influenza virus infections of mice. PloS One. 2011 Mar
973 14;6(3):e17618.
974 80. Tate MD, Deng Y-M, Jones JE, Anderson GP, Brooks AG, Reading PC.
975 Neutrophils ameliorate lung injury and the development of severe disease during influenza
976 infection. J Immunol Baltim Md 1950. 2009 Dec 1;183(11):7441–50.
977 81. Guilliams M, Mildner A, Yona S. Developmental and Functional Heterogeneity of
978 Monocytes. Immunity. 2018 Oct 16;49(4):595–613.
979 82. Short KR, Kroeze EJBV, Fouchier RAM, Kuiken T. Pathogenesis of influenza-
980 induced acute respiratory distress syndrome. Lancet Infect Dis. 2014 Jan;14(1):57–69.
981 83. Coillard A, Segura E. In vivo Differentiation of Human Monocytes. Front Immunol.
982 2019;10:1907.
983 84. Duan M, Hibbs ML, Chen W. The contributions of lung macrophage and monocyte
984 heterogeneity to influenza pathogenesis. Immunol Cell Biol. 2017 Mar;95(3):225–35.
985 85. Lim K, Kim T-H, Trzeciak A, Amitrano AM, Reilly EC, Prizant H, et al. In situ
986 neutrophil efferocytosis shapes T cell immunity to influenza infection. Nat Immunol. 2020
987 Sep;21(9):1046–57.
988 86. Dawson TC, Beck MA, Kuziel WA, Henderson F, Maeda N. Contrasting effects of
989 CCR5 and CCR2 deficiency in the pulmonary inflammatory response to influenza A virus.
990 Am J Pathol. 2000 Jun;156(6):1951–9.
991 87. Herold S, Steinmueller M, von Wulffen W, Cakarova L, Pinto R, Pleschka S, et al.
992 Lung epithelial apoptosis in influenza virus pneumonia: the role of macrophage-expressed
993 TNF-related apoptosis-inducing ligand. J Exp Med. 2008 Dec 22;205(13):3065–77.
994 88. Lin KL, Suzuki Y, Nakano H, Ramsburg E, Gunn MD. CCR2+ monocyte-derived
995 dendritic cells and exudate macrophages produce influenza-induced pulmonary immune
996 pathology and mortality. J Immunol Baltim Md 1950. 2008 Feb 15;180(4):2562–72.
997 89. Bar-On Y, Seidel E, Tsukerman P, Mandelboim M, Mandelboim O. Influenza virus
998 uses its neuraminidase protein to evade the recognition of two activating NK cell receptors.
999 J Infect Dis. 2014 Aug 1;210(3):410–8.
1000 90. Duev-Cohen A, Bar-On Y, Glasner A, Berhani O, Ophir Y, Levi-Schaffer F, et al.
1001 The human 2B4 and NTB-A receptors bind the influenza viral hemagglutinin and co-
1002 stimulate NK cell cytotoxicity. Oncotarget. 2016 Mar 15;7(11):13093–105.
1003 91. Ohkura T, Momose F, Ichikawa R, Takeuchi K, Morikawa Y. Influenza A virus
1004 hemagglutinin and neuraminidase mutually accelerate their apical targeting through
1005 clustering of lipid rafts. J Virol. 2014 Sep 1;88(17):10039–55.
1006 92. Miwa T, Maldonado MA, Zhou L, Yamada K, Gilkeson GS, Eisenberg RA, et al.
1007 Decay-accelerating factor ameliorates systemic autoimmune disease in MRL/lpr mice via
1008 both complement-dependent and -independent mechanisms. Am J Pathol. 2007
1009 Apr;170(4):1258–66.
1010 93. Miwa T, Maldonado MA, Zhou L, Sun X, Luo HY, Cai D, et al. Deletion of decay-
1011 accelerating factor (CD55) exacerbates autoimmune disease development in MRL/lpr
1012 mice. Am J Pathol. 2002 Sep;161(3):1077–86.
1013 94. Soltys J, Halperin JA, Xuebin Q. DAF/CD55 and Protectin/CD59 modulate adaptive
1014 immunity and disease outcome in experimental autoimmune myasthenia gravis. J

Neuroimmunol. 2012 Mar;244(1–2):63–9.
95. Varki A, Gagneux P. Multifarious roles of sialic acids in immunity. Ann N Y Acad Sci. 2012 Apr;1253:16–36.
96. Patel MC, Shirey KA, Boukhvalova MS, Vogel SN, Blanco JCG. Serum High-Mobility-Group Box 1 as a Biomarker and a Therapeutic Target during Respiratory Virus Infections. mBio. 2018 Mar 13;9(2).
97. Marjuki H, Mishin VP, Chesnokov AP, De La Cruz JA, Fry AM, Villanueva J, et al. An investigational antiviral drug, DAS181, effectively inhibits replication of zoonotic influenza A virus subtype H7N9 and protects mice from lethality. J Infect Dis. 2014 Aug 1;210(3):435–40.
98. Hariri BM, Cohen NA. New insights into upper airway innate immunity. Am J Rhinol Allergy. 2016 Sep;30(5):319–23.
99. Zanin M, Baviskar P, Webster R, Webby R. The Interaction between Respiratory Pathogens and Mucus. Cell Host Microbe. 2016 Feb 10;19(2):159–68.
100. Gaush CR, Smith TF. Replication and plaque assay of influenza virus in an established line of canine kidney cells. Appl Microbiol. 1968 Apr;16(4):588–94.
101. Matrosovich M, Matrosovich T, Garten W, Klenk H-D. New low-viscosity overlay medium for viral plaque assays. Virol J. 2006 Aug 31;3:63.
102. Amorim MJ, Bruce EA, Read EKC, Foeglein A, Mahen R, Stuart AD, et al. A Rab11- and microtubule-dependent mechanism for cytoplasmic transport of influenza A virus viral RNA. J Virol. 2011 May;85(9):4143–56.
103. Moskovich O, Fishelson Z. Quantification of complement C5b-9 binding to cells by flow cytometry. Methods Mol Biol Clifton NJ. 2014;1100:103–8.
104. Durkin ME, Qian X, Popescu NC, Lowy DR. Isolation of Mouse Embryo Fibroblasts. Bio-Protoc. 2013 Sep 20;3(18).
105. Hoffmann E, Neumann G, Kawaoka Y, Hobom G, Webster RG. A DNA transfection system for generation of influenza A virus from eight plasmids. Proc Natl Acad Sci U S A. 2000 May 23;97(11):6108–13.
106. James J, Howard W, Iqbal M, Nair VK, Barclay WS, Shelton H. Influenza A virus PB1-F2 protein prolongs viral shedding in chickens lengthening the transmission window. J Gen Virol. 2016 Oct;97(10):2516–27.
107. Bialy D, Shelton H. Functional neuraminidase inhibitor resistance motifs in avian influenza A(H5Nx) viruses. Antiviral Res. 2020 Oct;182:104886.
108. Chang P, Sealy JE, Sadeyen J-R, Bhat S, Lukosaityte D, Sun Y, et al. Immune Escape Adaptive Mutations in the H7N9 Avian Influenza Hemagglutinin Protein Increase Virus Replication Fitness and Decrease Pandemic Potential. J Virol. 2020 Sep 15;94(19).
109. de Wit E, Spronken MIJ, Vervaet G, Rimmelzwaan GF, Osterhaus ADME, Fouchier RAM. A reverse-genetics system for Influenza A virus using T7 RNA polymerase. J Gen Virol. 2007 Apr;88(Pt 4):1281–7.
110. de Wit E, Spronken MIJ, Bestebroer TM, Rimmelzwaan GF, Osterhaus ADME, Fouchier RAM. Efficient generation and growth of influenza virus A/PR/8/34 from eight cDNA fragments. Virus Res. 2004 Jul;103(1–2):155–61.

Author contributions

Conceptualization: NBS, ZEVS, MJA; Funding acquisition: MJA; Investigation: NBS, ZEVS, CG, CAR; Supervision: MJA; Visualization: NBS, ZEVS, MJA; Writing: NBS, ZEVS, MJA.

Acknowledgements

We acknowledge Dr. Colin Adrain (IGC, Portugal), Dr. Holly Shelton (The Pirbright Institute, UK), Dr. Jonathan Yewdell (NIAID, USA), Dr. Luís Moita (IGC, Portugal), Dr. Miguel Soares (IGC, Portugal), Prof. Paul Digard (Roslin Institute, UK), Dr. Ron Fouchier (Erasmus, Netherlands), Dr. Vera Martins and Prof. Wen-Chao Song (University of Pennsylvania, USA) for providing mice, cells and reagents. We are grateful to the Animal House Facility, Flow Cytometry Facility and Histopathology Unit at the IGC for technical support, sample processing and data collection. We thank André Barros (IGC Portugal), Dr. Mónica Bettencourt-Dias (IGC, Portugal), Dr. Gabriel Nuñez (University of Michigan) and the members of CBV lab for helpful discussion.

Figure and table legends

Fig. 1 – Decay-accelerating factor (DAF) aggravates IAV infection *in vivo.*

A, B: Bodyweight loss (**A**) and mortality (**B**) of C57BL/6J WT or *Daf*$^{-/-}$ mice infected with 1000 PFU of A/California/7/2009 (Cal) (Inf n = 8; mock n = 3 for per group) **C, D**: Bodyweight loss (**C**) and mortality (**D**) of C57BL/6J WT or *Daf*$^{-/-}$ mice infected with 1000 PFU of A/England/195/2009 (Eng) (Inf n = 9 per group; mock n = 5 and n = 4 for WT and *Daf*$^{-/-}$ respectively). Results are expressed as mean±sd, statistical analysis detailed in materials and methods.

Fig. 2 – *Daf*$^{-/-}$ mice are protected against PR8-HK4,6, but not PR8, and protection is specific of this RCA.

A, B: Bodyweight loss (**A**) and mortality (**B**) of C57BL/6J WT or *Daf*$^{-/-}$ mice infected with the indicated doses of A/Puerto Rico/8/1934 (PR8) (**A**: Inf n = 8 per group; mock n = 7 and n = 4 for WT and *Daf*$^{-/-}$ respectively; **B**: Inf n = 9 and n = 10, mock n = 8 and n = 4 for WT and *Daf*$^{-/-}$ respectively). **C, D**: Bodyweight loss (**C**) and mortality (**D**) of C57BL/6J WT or *Daf*$^{-/-}$ mice infected with the indicated doses of A/X-31 (PR8-HK4,6) (**C:** Inf n = 9 and n = 10, mock n = 8 and n = 4 for WT and *Daf*$^{-/-}$ respectively; **D:** Inf n = 7 and n = 8, mock n = 3 and n = 2 for WT and *Daf*$^{-/-}$ respectively). **E, F**: Bodyweight loss (**E**) and mortality (**F**) of C57BL/6J WT or *Cd59*$^{-/-}$ mice infected with the indicated doses of PR8-HK4,6 (**E:** Inf n = 10 and n = 11 for WT and *Daf*$^{-/-}$ respectively, mock = 7 per group; **F**: Inf n = 10 per group, mock n = 4 and n = 7 for WT and *Daf*$^{-/-}$ respectively). Results are expressed as mean±sd, statistical analysis detailed in materials and methods.

Fig. 3 – DAF does not affect viral replication, clearance, or tissue penetration, but is an immunopathology instigator.

A, B: Lung viral titers of C57BL/6J WT or *Daf*$^{-/-}$ mice infected with 1000 PFU of A/X-31 (PR8HK4,6). Samples collected at 3 d.p.i. (**A,** n = 13 and n = 14 for WT and *Daf*$^{-/-}$ respectively) and 6 d.p.i. (**B,** n = 18 and n = 19 for WT and *Daf*$^{-/-}$ respectively). **C**: Immunohistochemistry detection of IAV nucleoprotein (NP) in WT or *Daf*$^{-/-}$ mice 3 d.p.i. with 1000 PFU of PR8HK4,6 (+ healthy; + infected). **D**: Quantification of infected bronchioli (n = 6 per group). **E, F**: Histological score of C57BL/6J WT or *Daf*$^{-/-}$ mice infected with 1000 PFU of PR8HK4,6 was assessed blindly. Evaluated parameters detailed in Table S1. Samples collected at 3 d.p.i. (**E,** n = 11 and n = 10 for WT and *Daf*$^{-/-}$ respectively) and 6 d.p.i. (**F,** n = 15 per group). Results are expressed as mean±sd. Statistical analysis detailed in materials and methods.

Fig. 4 – *Daf*$^{-/-}$ mice have reduced complement activation and recruitment of innate immune cells.

A: Bodyweight loss of C57BL/6J WT, *C3*$^{-/-}$ or *C3*$^{-/-}$ / *Daf*$^{-/-}$ mice infected with 500 PFU of A/X-31 (PR8-HK4,6) (Inf n = 10, n = 6 and n = 10, mock n = 5, n = 5 and n = 7 for WT, *C3*$^{-/-}$ and *C3*$^{-/-}$ / *Daf*$^{-/-}$ respectively). Results are expressed as mean±sd. **B**: C3a levels in BALs of C57BL/6J WT (n = 7) or *Daf*$^{-/-}$ (n = 8) mice 6 d.p.i. with 1000 PFU of PR8-HK4,6. Results are expressed as mean±sd. **C:** Cell death of primary lung cells derived from WT or *Daf*$^{-/-}$ mice infected or mock-infected with PR8-HK4,6 and treated with serum. Results are expressed as mean±sd from 3 replicates from 2 independent experiments. **D, E, F**: Analysis of NK cells (**D**, n = 6 and n = 3 for WT and *Daf*$^{-/-}$ respectively), neutrophils (**E**, n = 11 and n = 10 for WT and *Daf*$^{-/-}$ respectively) and monocytes (**F,** n = 11 and n = 10 for WT and *Daf*$^{-/-}$ respectively) levels in BALs of WT or *Daf*$^{-/-}$ mice, 3 d.p.i. with 1000 PFU PR8-HK4,6. Results are expressed as mean±sd. **G, H, I, J, K**: Analysis of neutrophils (**G**), monocytes (**H**), CD4^{+} T cells (**I**), CD8^{+} T cells (**J**) and IFN-γ (**K**) levels in BALs of WT or

Daf$^{-/-}$ mice, 6 d.p.i. with 1000 PFU PR8-HK4,6 (n = 10 per group). Results are expressed as mean±sd. Statistical analysis detailed in materials and methods.

Fig. 5 – DAF interaction with HA worsens disease outcome, without increasing immunopathology.

A, B: Bodyweight loss (**A**) and mortality (**B**) of C57BL/6J WT or *Daf*$^{-/-}$ mice infected with the indicated doses of A/Puerto Rico/8/1934 with segment 6 from A/Hong Kong/1/68 (PR8-HK6). (**A:** Inf n = 16 and n = 18, mock n = 6 and n = 7 for WT and *Daf*$^{-/-}$ respectively; **B:** Inf n = 12 and n = 9, mock n = 4 and n = 2 for WT and *Daf*$^{-/-}$ respectively). Results are expressed as mean±sd. **C, D**: Lung viral titers of C57BL/6J WT or *Daf*$^{-/-}$ mice infected with 20 PFU of PR8-HK6. Samples collected at 3 d.p.i. (**C**) and 6 d.p.i. (**D**) (n = 10 and n = 7 for WT and *Daf*$^{-/-}$ respectively). **E**: Immunohistochemistry detection of IAV nucleoprotein (NP) in WT or *Daf*$^{-/-}$ 3 d.p.i. with 20 PFU of PR8-HK6 (+ healthy; + infected). **F**: Quantification of infected bronchioli (n = 5 per group). **G, H**: Histological score of C57BL/6J WT or *Daf*$^{-/-}$ mice infected with 20 PFU of PR8HK-6. Samples collected at 3 d.p.i. (**E,** n = 10 and n = 7 for WT and *Daf*$^{-/-}$ respectively) and 6 d.p.i. (**F**, n = 10 and n = 8 for WT and *Daf*$^{-/-}$ respectively). Results are expressed as mean±sd. Statistical analysis detailed in materials and methods.

Fig. 6 – *Daf*$^{-/-}$ mice have reduced complement activation and T cell recruitment upon PR8-HK6 infection.

A: Bodyweight loss of C57BL/6J WT *C3*$^{-/-}$ or *C3*$^{-/-}$ / *Daf*$^{-/-}$ mice infected with 20 PFU of A/Puerto Rico/8/1934 with segment 6 from A/Hong Kong/1/68 (PR8-HK6) (Inf n = 10, n = 10 and n = 4, mock n = 4, n = 3 and n = 1, for WT, *C3*$^{-/-}$ and *C3*$^{-/-}$ / *Daf*$^{-/-}$ respectively). Results are expressed as mean±sd. **B**: C3a levels in BALs of C57BL/6J WT (n = 10) or *Daf*$^{-/-}$ (n = 8) mice 6 d.p.i. with 20 PFU of PR8-HK6. Results are expressed as mean±sd. **C,**

D: Analysis of neutrophils (**C**) and monocytes (**D**) levels in BALs of WT (n = 7) or *Daf*$^{-/-}$ (n = 6) mice, 3 d.p.i. with 10 PFU PR8-HK6. Results are expressed as mean±sd. **E, F, G, H**: Analysis of neutrophils (**E**), monocyte (**F**), CD4^{+} T cells (**G**) and CD8^{+} T cells (**H**) levels in BALs of WT (n = 10) or *Daf*$^{-/-}$ (n = 8) mice, 6 d.p.i. with 20 PFU PR8-HK6. Results are expressed as mean±sd. Statistical analysis detailed in materials and methods.

Fig. 7 – DAF interaction with NA modulates immunopathology.

A, B: Bodyweight loss (**A**) and mortality (**B**) of C57BL/6J WT or *Daf*$^{-/-}$ mice infected with the indicated doses of A/Puerto Rico/8/1934 with segment 4 from A/Hong Kong/1/68 (PR8-HK4). (**A**: Inf n = 14 and n = 10, mock n = 4 and n = 1 for WT and *Daf*$^{-/-}$ respectively; **B:** Inf n = 8 per group, mock n = 4 and n = 1 for WT and *Daf*$^{-/-}$ respectively). Results are expressed as mean±sd**. C, D**: Lung viral titers of C57BL/6J WT or *Daf*$^{-/-}$ mice infected with 100 PFU of PR8-HK4. Samples collected at 3 d.p.i. (**C,** n = 9 and n = 8 for WT and *Daf*$^{-/-}$ respectively) and 6 d.p.i. (**D,** n = 9 per group). Results are expressed as mean±sd. **E**: Immunohistochemistry detection of IAV nucleoprotein (NP) in WT or *Daf*$^{-/-}$ 3 d.p.i. with 100 PFU of PR8-HK4 (+ healthy; + infected). **F**: Quantification of infected bronchioli (n = 5 per group). **G, H**: Histological score of C57BL/6J WT or *Daf*$^{-/-}$ mice infected with 100 PFU of PR8-HK4. Samples collected at 3 d.p.i. (**G,** Inf n = 16 and n = 18, mock n = 6 and n = 7 for WT and *Daf*$^{-/-}$ respectively) and 6 d.p.i. (**H**, Inf n = 13 and n = 9, mock n = 4 and n = 2 for WT and *Daf*$^{-/-}$ respectively). Results are expressed as mean±sd. Statistical analysis detailed in materials and methods.

Fig. 8 – *Daf*$^{-/-}$ mice present lower complement activation and neutrophil recruitment at 3 d.p.i. upon PR8-HK4 infection.

A: Bodyweight loss of C57BL/6J WT *C3*$^{-/-}$ or *C3*$^{-/-}$ / *Daf*$^{-/-}$ mice infected with 100 PFU of A/Puerto Rico/8/1934 with segment 4 from A/Hong Kong/1/68 (PR8-HK4) (Inf n =

14, n = 10, and n = 3, mock n = 4, n = 3 and n = 1 for WT, *C3*$^{-/-}$ and *C3*$^{-/-}$ / *Daf*$^{-/-}$ respectively). Results are expressed as mean±sd. **B**: C3a levels in BALs of C57BL/6J WT or *Daf*$^{-/-}$ mice 6 d.p.i. with 100 PFU of PR8-HK4 (n = 9 per group). Results are expressed as mean±sd. **C, D**: Analysis of neutrophils (**C**) and monocytes (**D**) levels in BALs of WT or *Daf*$^{-/-}$ mice, 3 d.p.i. with 100 PFU PR8-HK4 (n = 6 per group). Results are expressed as mean±sd. **E, F, G, H**: Analysis of neutrophils (**E**), monocyte (**F**), CD4^{+} T cells (**G**) and CD8^{+} T cells (**H**) levels in BALs of WT or *Daf*$^{-/-}$ mice, 6 d.p.i. with 100 PFU PR8-HK4 (n = 9 per group). Results are expressed as mean±sd. Statistical analysis detailed in materials and methods.

Fig. 9 – Influenza A virus neuraminidase cleaves DAF through its sialidase activity.

A: Western blot detection of complement decay-accelerating factor (DAF) in A549 cells upon infection with A/California/7/2009 (Cal), A/England/195/2009 (Eng), A/Puerto Rico/8/1934 (PR8) or A/X-31 (PR8-HK4,6) at a multiplicity of infection (MOI) of 5. **B:** The proportion of cleaved DAF was measured in each lane as the ratio of low molecular weight (MW) to total DAF pixel densitometry. **C:** Western blot detection of DAF in mouse embryonic fibroblasts (MEFs) derived from C57/BL6 WT or *Daf*$^{-/-}$ mice upon infection with PR8 or PR8-HK4,6 at a MOI of 5. **D:** The proportion of cleaved DAF was measured in each lane as the ratio of low MW to total DAF pixel densitometry. (**B**, **D**: data shown as mean±sd, from three independent experiments). **E:** Western blot detection of DAF in HEK293T cells after transfection with plasmids encoding the eight different PR8 viral segments. **F:** Western blot detection of DAF in HEK293T cells transfected with eight plasmids encoding each of the PR8 segments, including wild-type NA (WT) or the catalytically-impaired mutant NA-E229A (E229A). **G:** Western blot detection of DAF in A549 cells upon infection with PR8 at a MOI of 5, treated with Zanamivir. **H:** The

proportion of cleaved DAF was measured in each lane as the ratio of low MW to total DAF pixel densitometry (data shown as mean±sd, from four independent experiments.) **I:** Flow cytometry detection of C5b-9 deposition in A549 cells after transduction with WT or catalytically-impaired mutant NA-E229A and treatment with serum (data shown as mean±sd, from six independent experiments, each corresponding to a pool of five independent transductions. Each point represents the median fluorescence intensity (MFI) of a sample treated with serum minus its corresponding heat-inactivated control.). **J:** DAF was purified by immunoprecipitation from cell lysates of A549 cells infected with PR8 at 12 hours post-infection (h.p.i.), treated with PNGaseF and analyzed by western blot or lectin blot with *Sambucus nigra* agglutinin (SNA) (* indicates IgGs from immunoprecipitation). Results are representative of three independent experiments. **K:** Western blot detection of DAF in HEK293T cells after transfection with plasmids encoding NAs from the indicated avian IAVs: H6N1 A/chicken/Taiwan/67/2013, H9N2 A/chicken/Pakistan/UDL-01/08, H5N2 A/goose/Taiwan/01031/2015, H5N6 A/chicken/Jiangxi/02.05 YGYXG023-P/2015, H4N6 A/chicken/Hunan/S1267/2010, H10N8 A/chicken/Jiangxi/1204/2014, H5N8 A/scarlet ibis/Germany/Ar44-L01279/2015, H7N9 A/Anhui/1/2013.

Yellow arrows indicate cleaved DAF. MW is indicated in kDa. Statistical analysis detailed in materials and methods.

Fig. 10 – Proposed model for DAF-mediated immunopathology.

At steady state, DAF accelerates the decay of C3 convertases, inhibiting the formation of C3a and C3b and subsequent complement activation. Upon IAV infection, the cell will produce viral proteins, and in particular NA. NA is a potent sialidase that will remove the sialic acid content of DAF both in the cytoplasm and at the surface. This processing of DAF by NA leads to DAF loss/alteration of function and hence overactivation of the complement pathway that will recruit innate immune cells. The excess of innate

immune response leads to tissue damage and ultimately immunopathology, worsening disease outcome.

Fig. 1

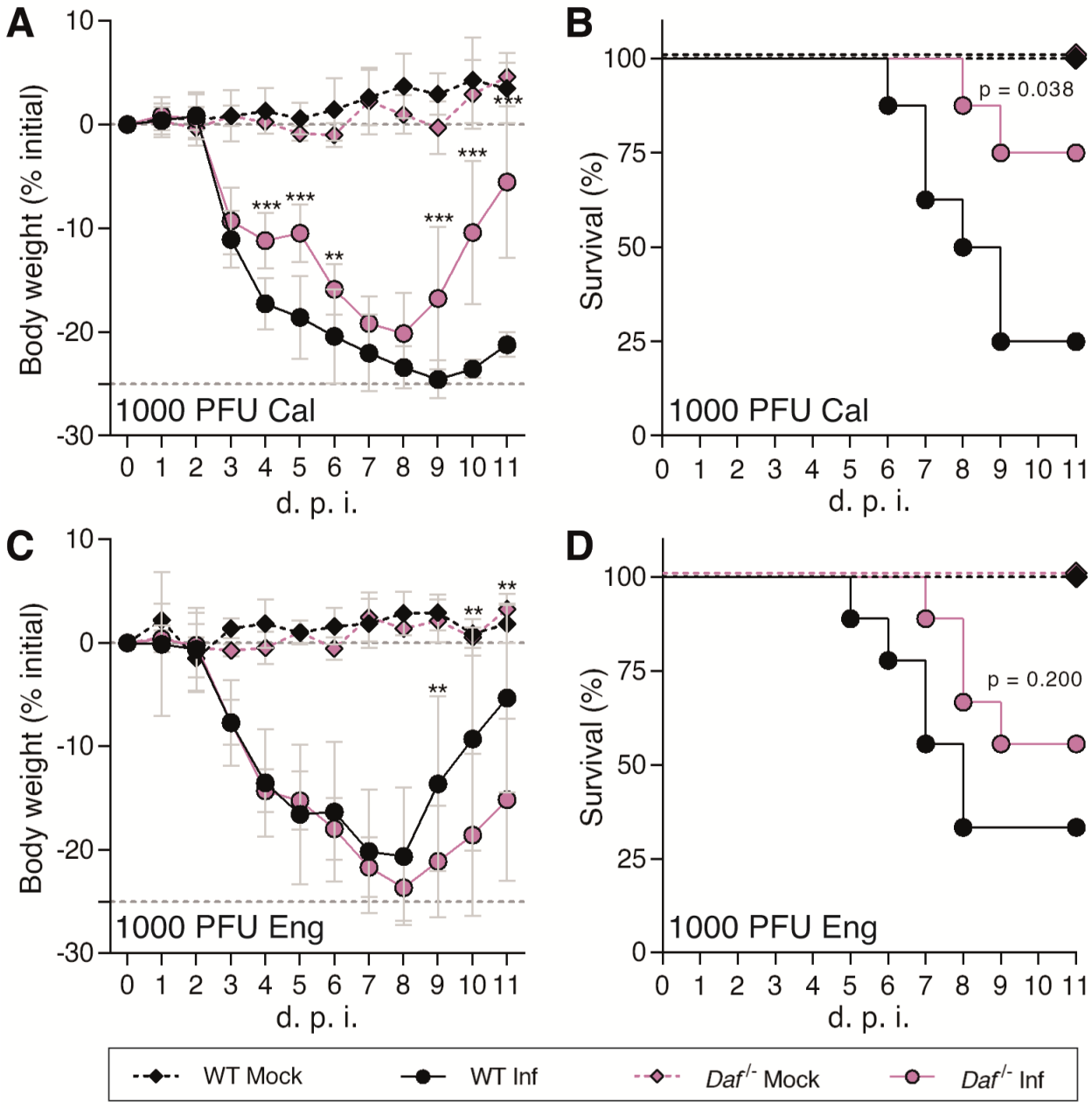

Fig. 2

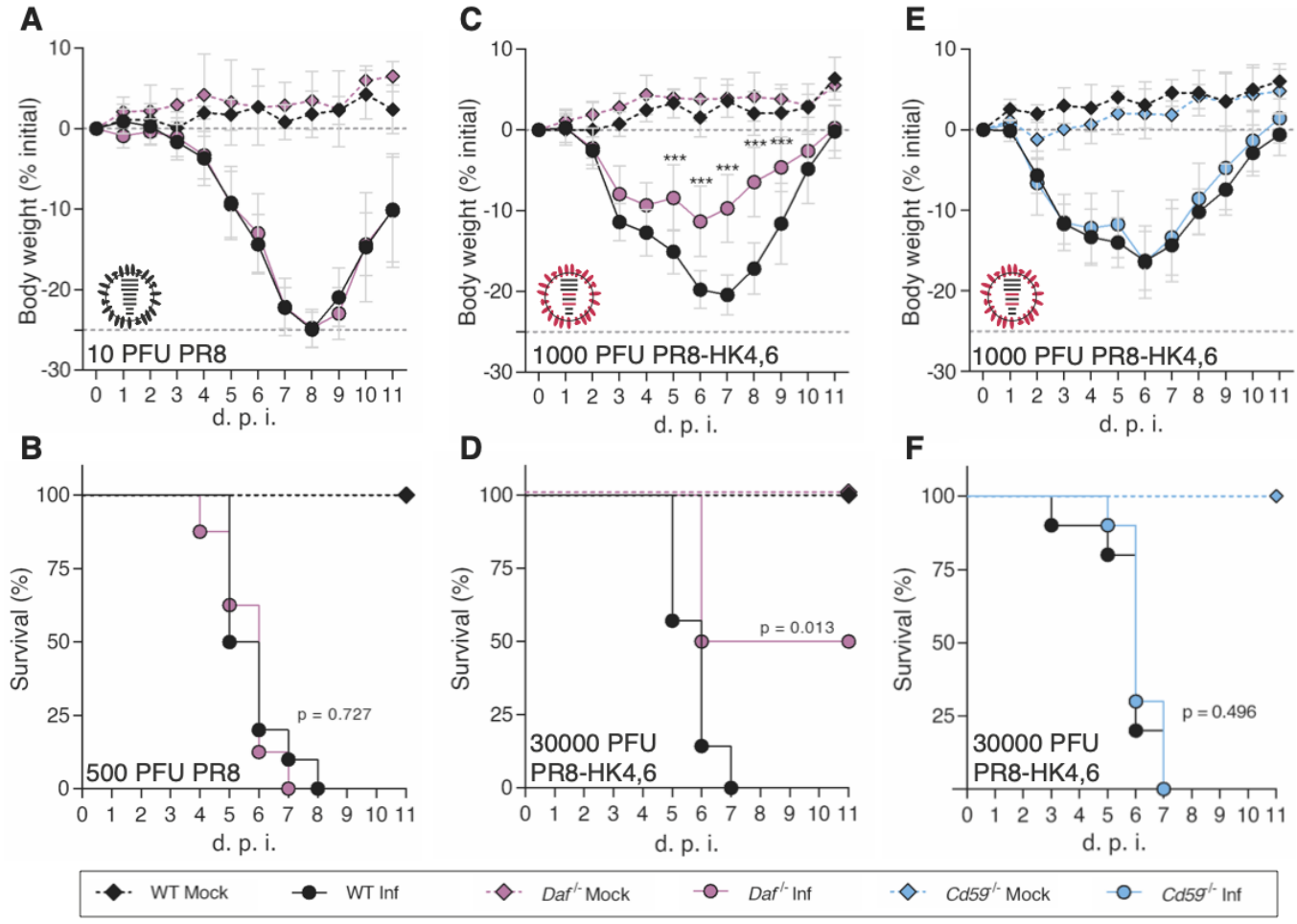

1241 **Fig. 3**

1242

1243

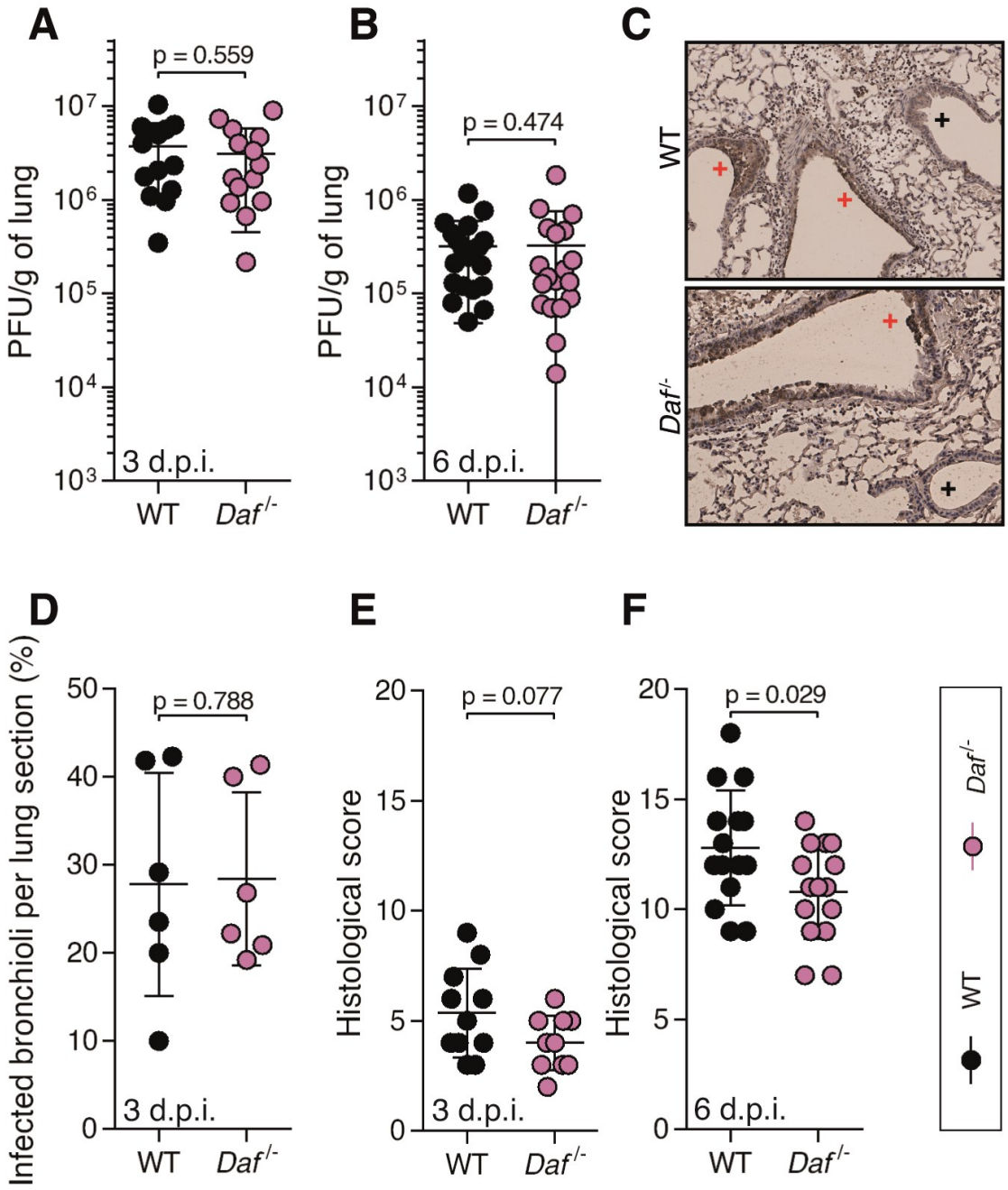

Fig. 4

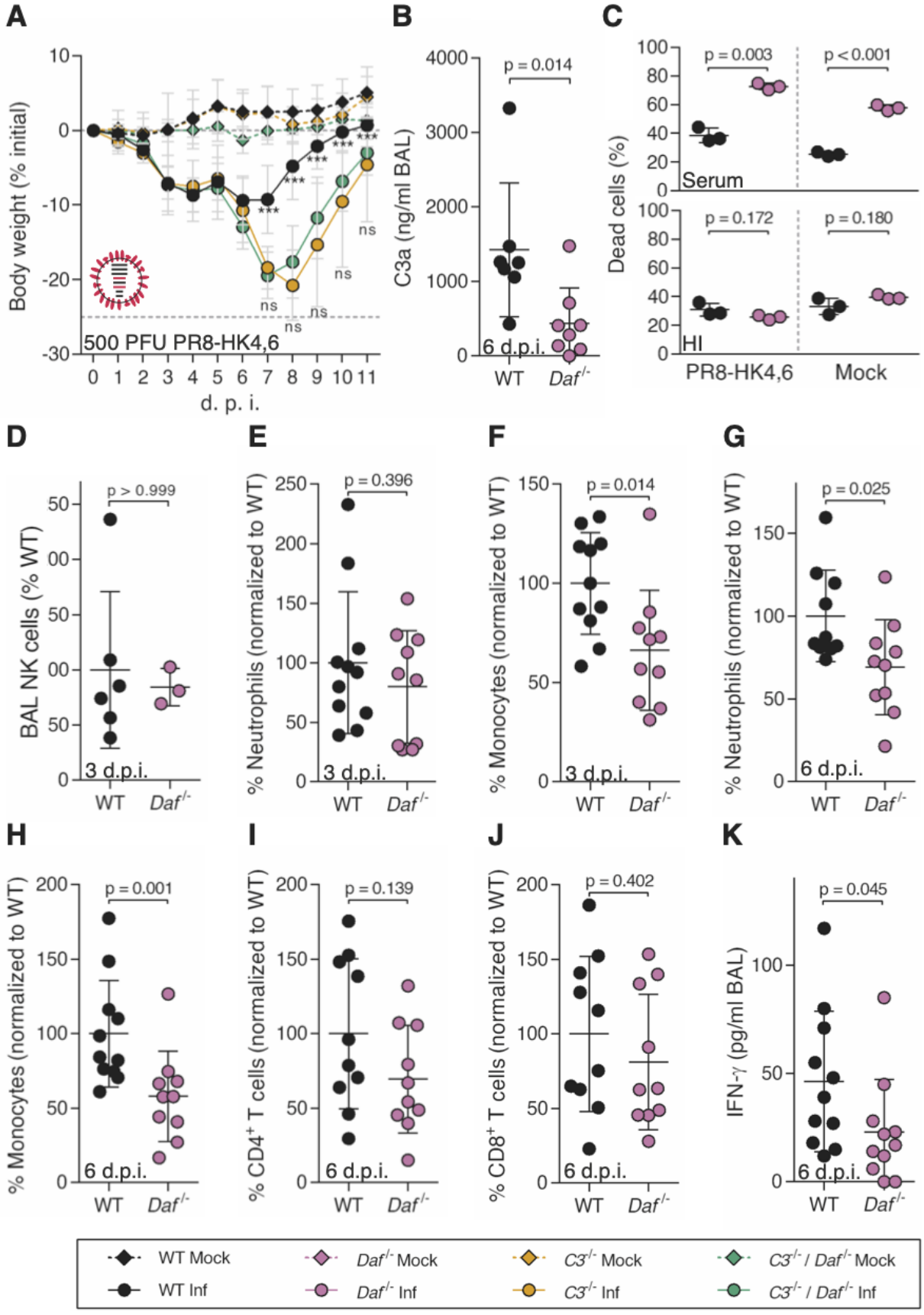

1247 **Fig. 5**

1248

1249

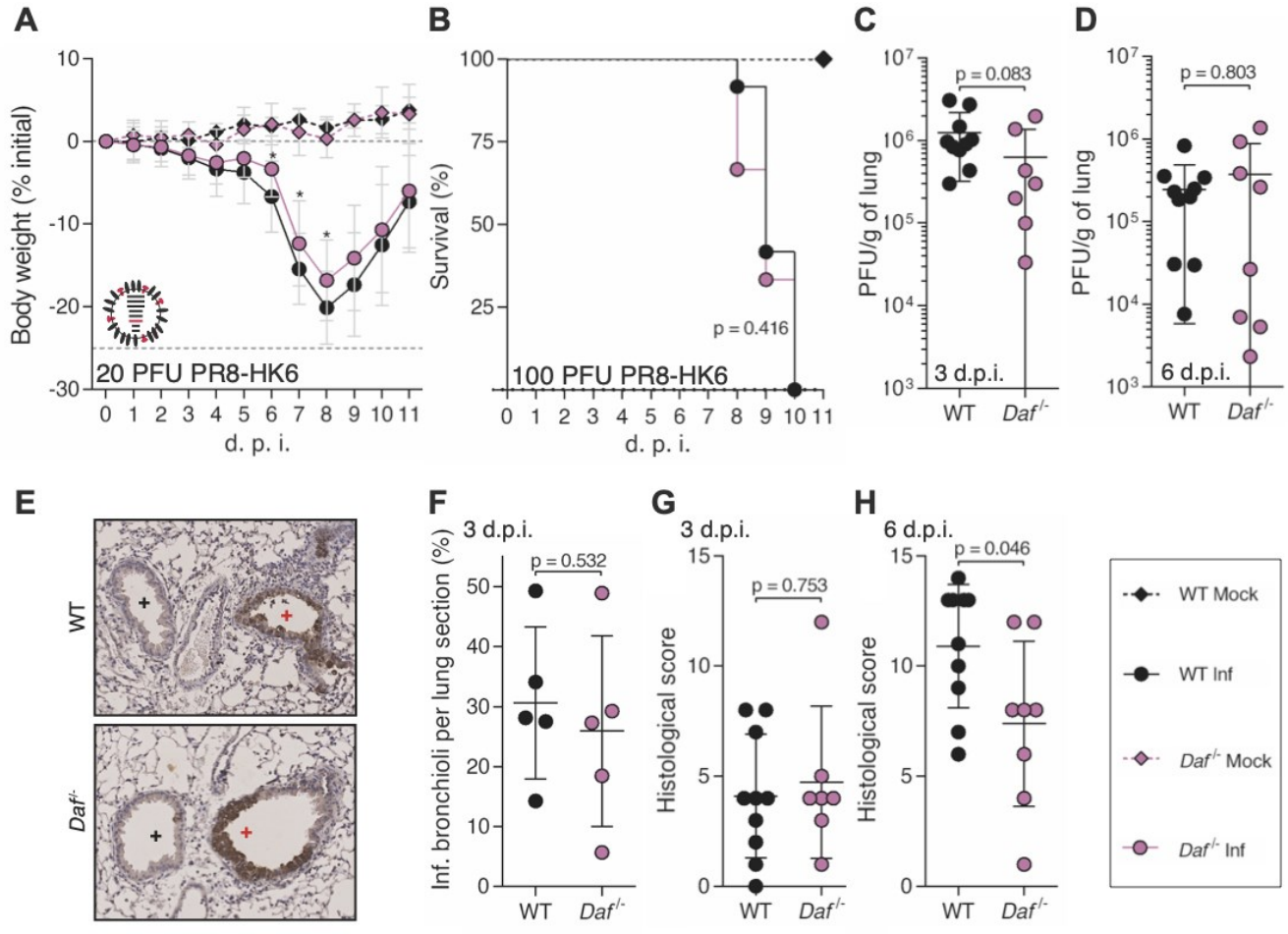

Fig. 6

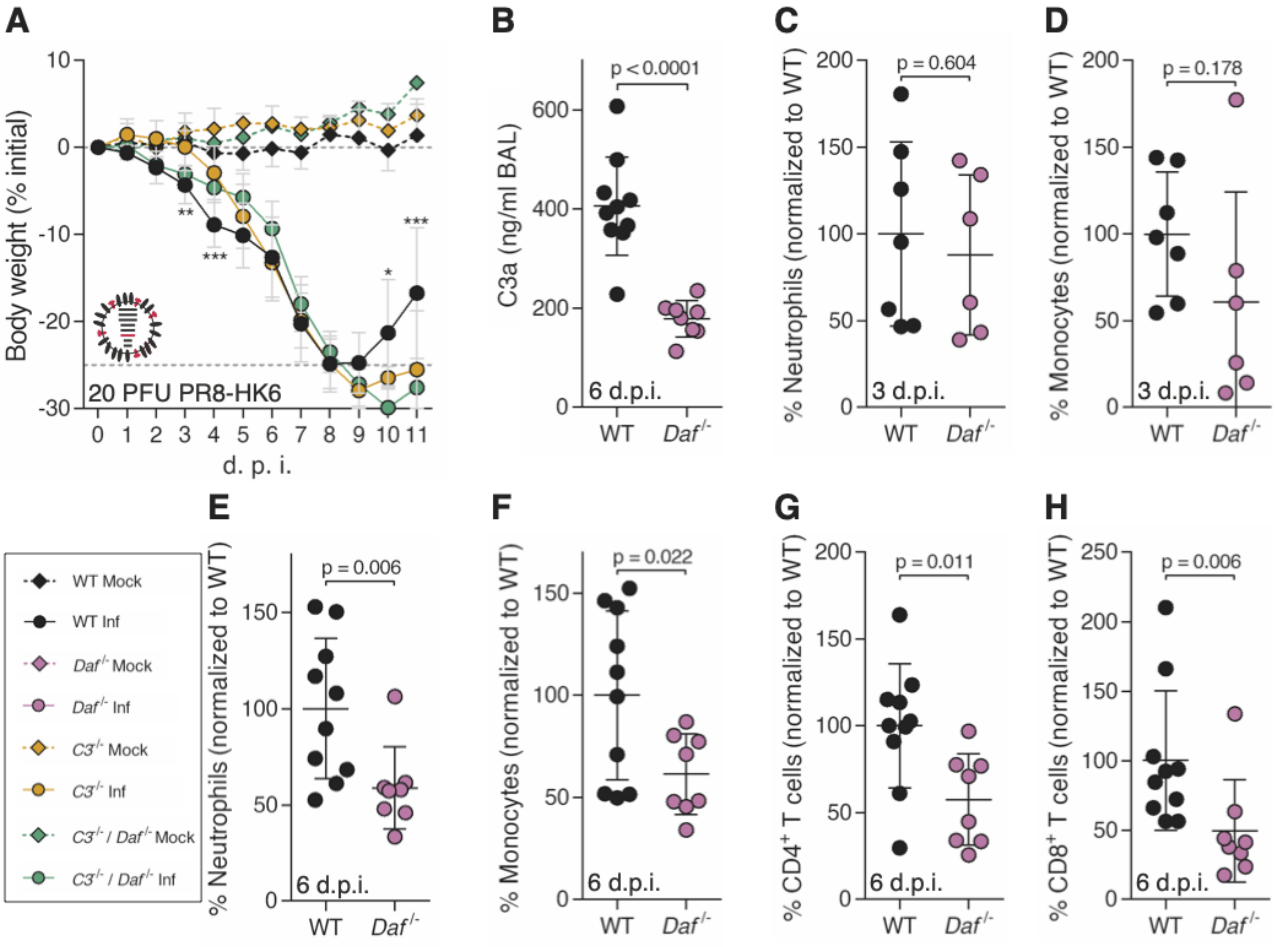

Fig. 7

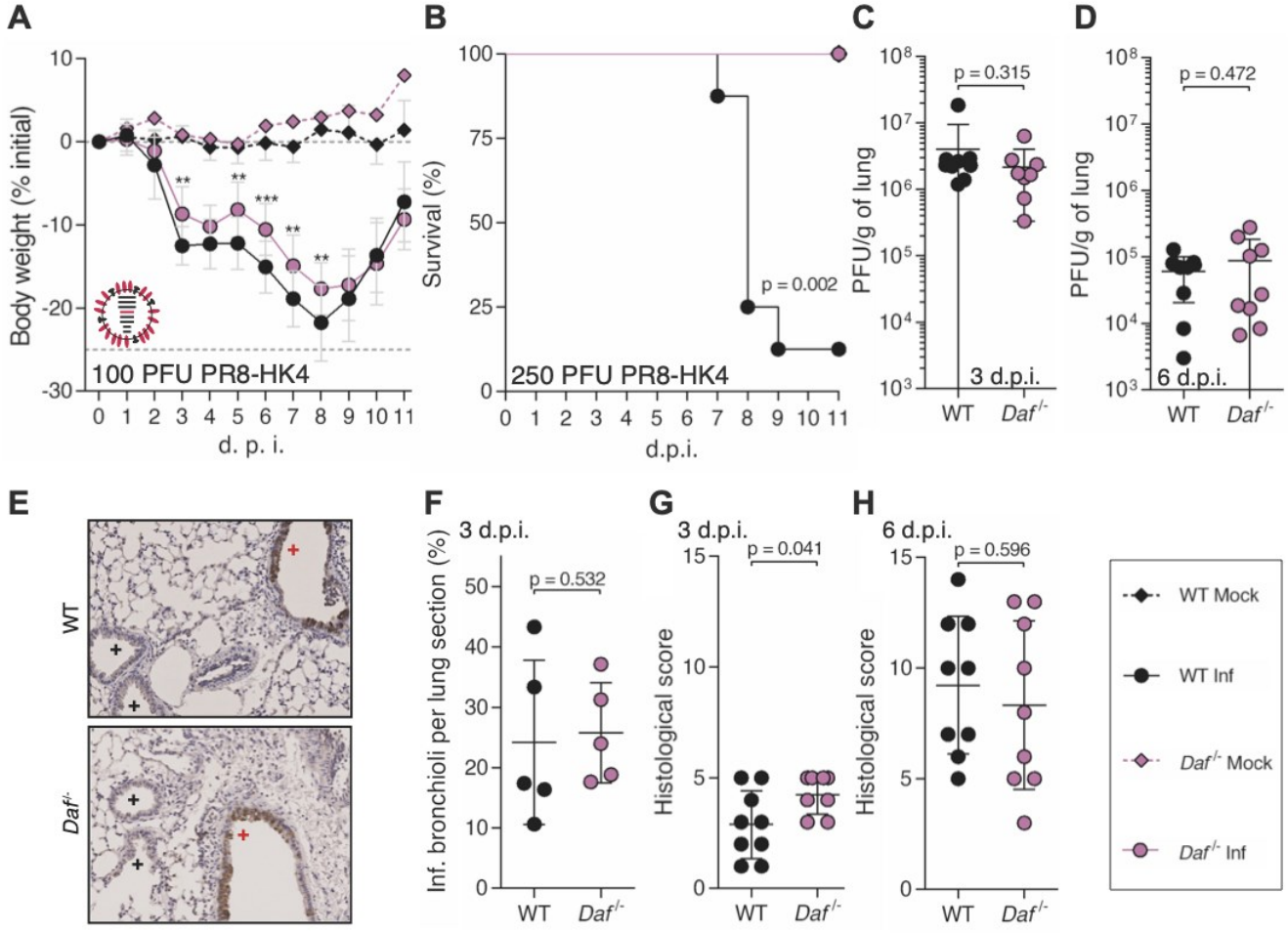

Fig. 8

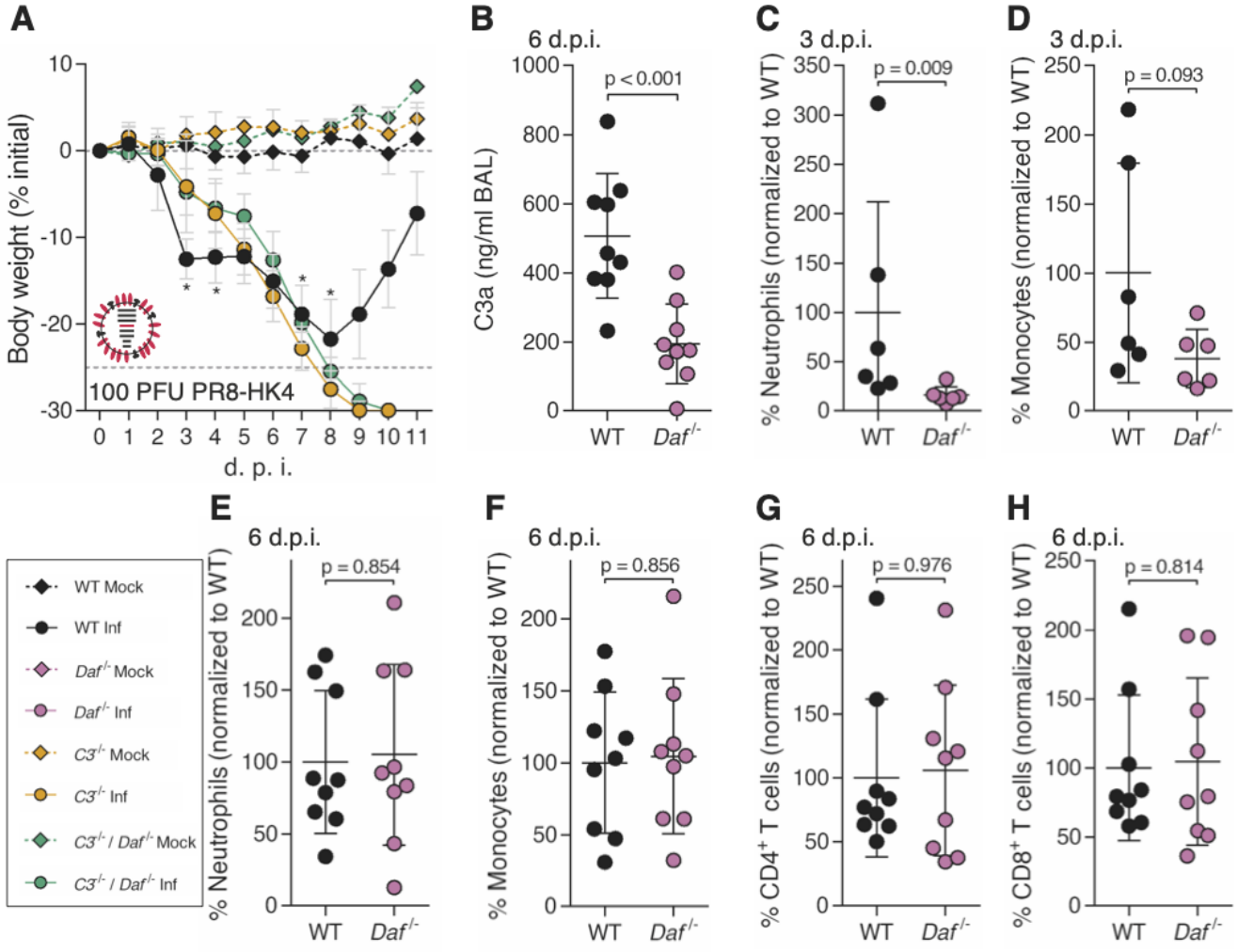

Fig. 9

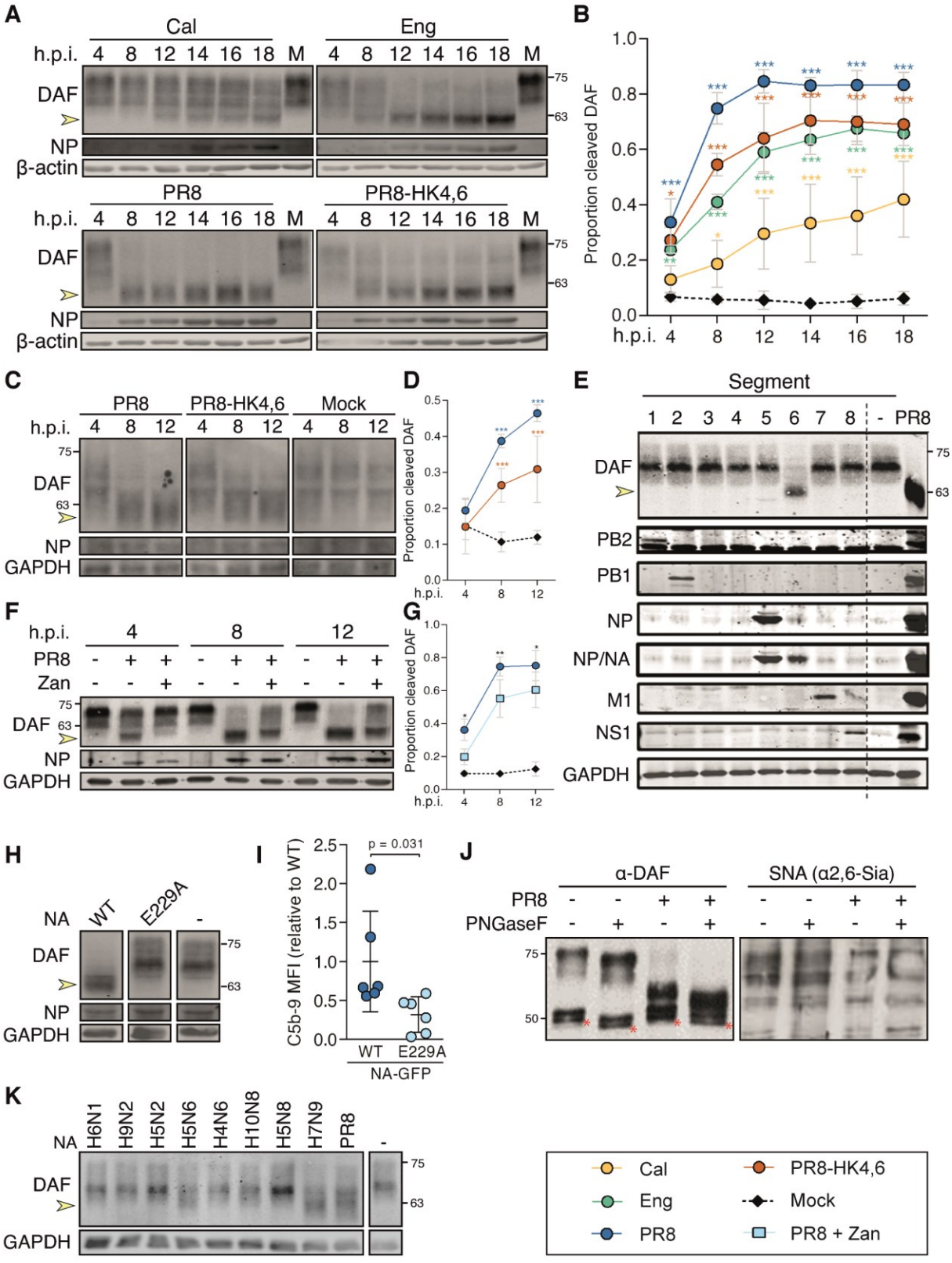

1262 **Fig. 10**

1263

1264

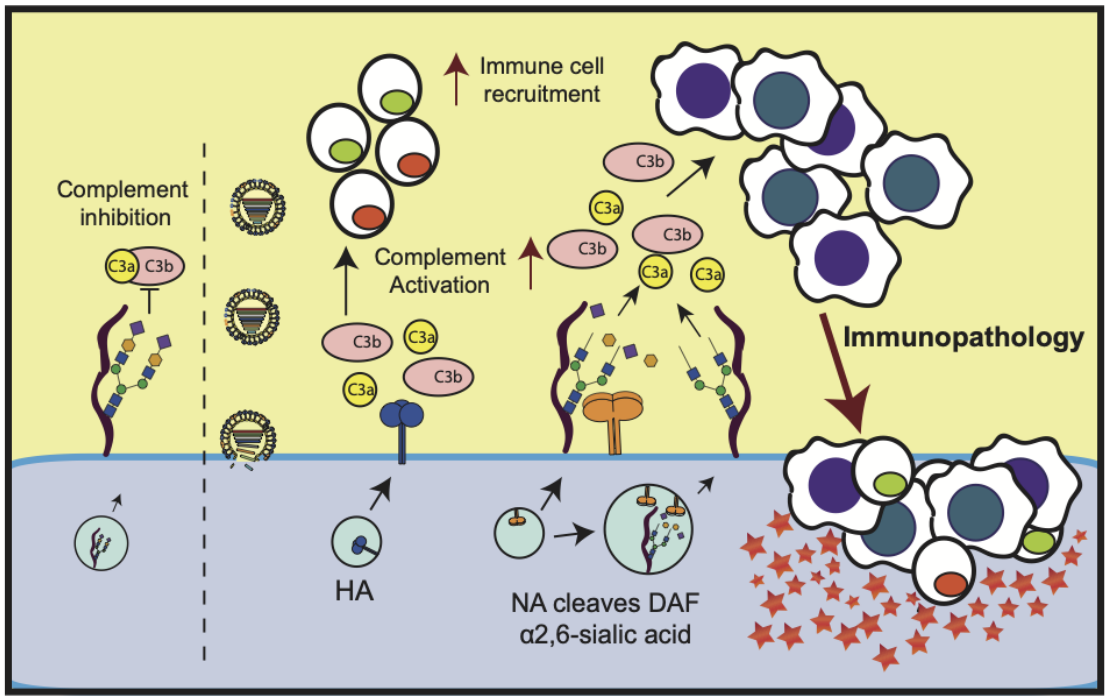

Supplementary material for Complement Decay-Accelerating Factor is a modulator of influenza A virus lung immunopathology

Nuno Brito Santos[1,6], Zoé Enderlin Vaz da Silva[1,6], Catarina Gomes[2,3], Celso A. Reis[2,3,4,5] and Maria João Amorim[1,*]

The supplementary material includes 3 supplementary figures and 3 tables.

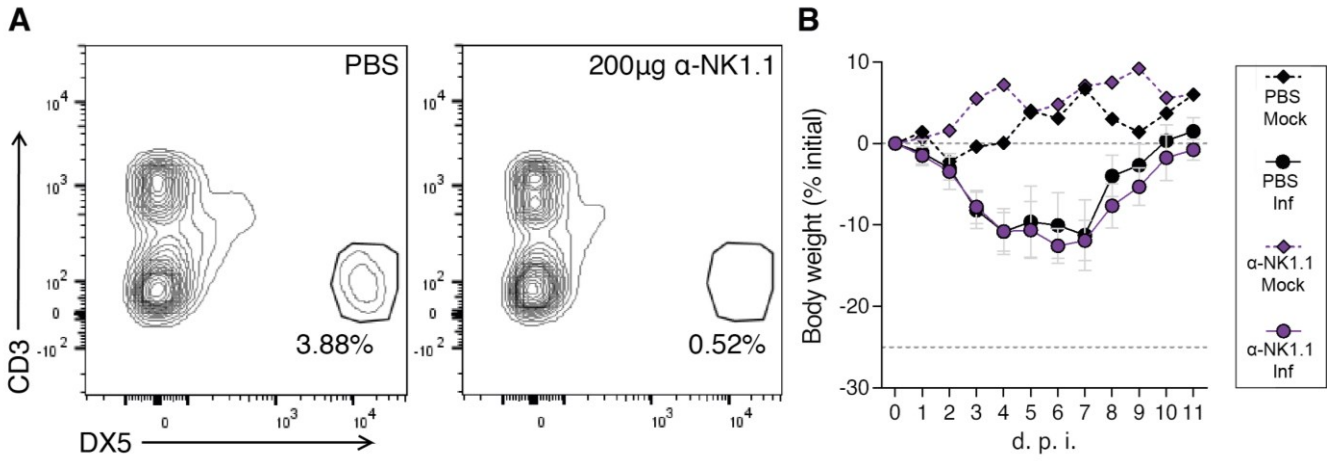

Fig. S1 – NK cell depletion does not alter disease outcome.

A: Representative flow cytometry detection of NK cells (gated in CD45$^+$ population) in C57BL/6J WT 72 hours after depletion via intraperitoneal (IP) injection of α-NK1.1. **B:** Bodyweight loss of C57BL/6J WT mice infected with 100 PFU of A/X-31 (PR8-HK4,6) and depleted of NK cells by IP injection of α-NK1.1 every 72 hours, starting 72 hours before infection (Inf n = 5 and mock n = 1 per group). Results are expressed as mean±sd. Statistical analysis detailed in materials and methods.

Fig. S2

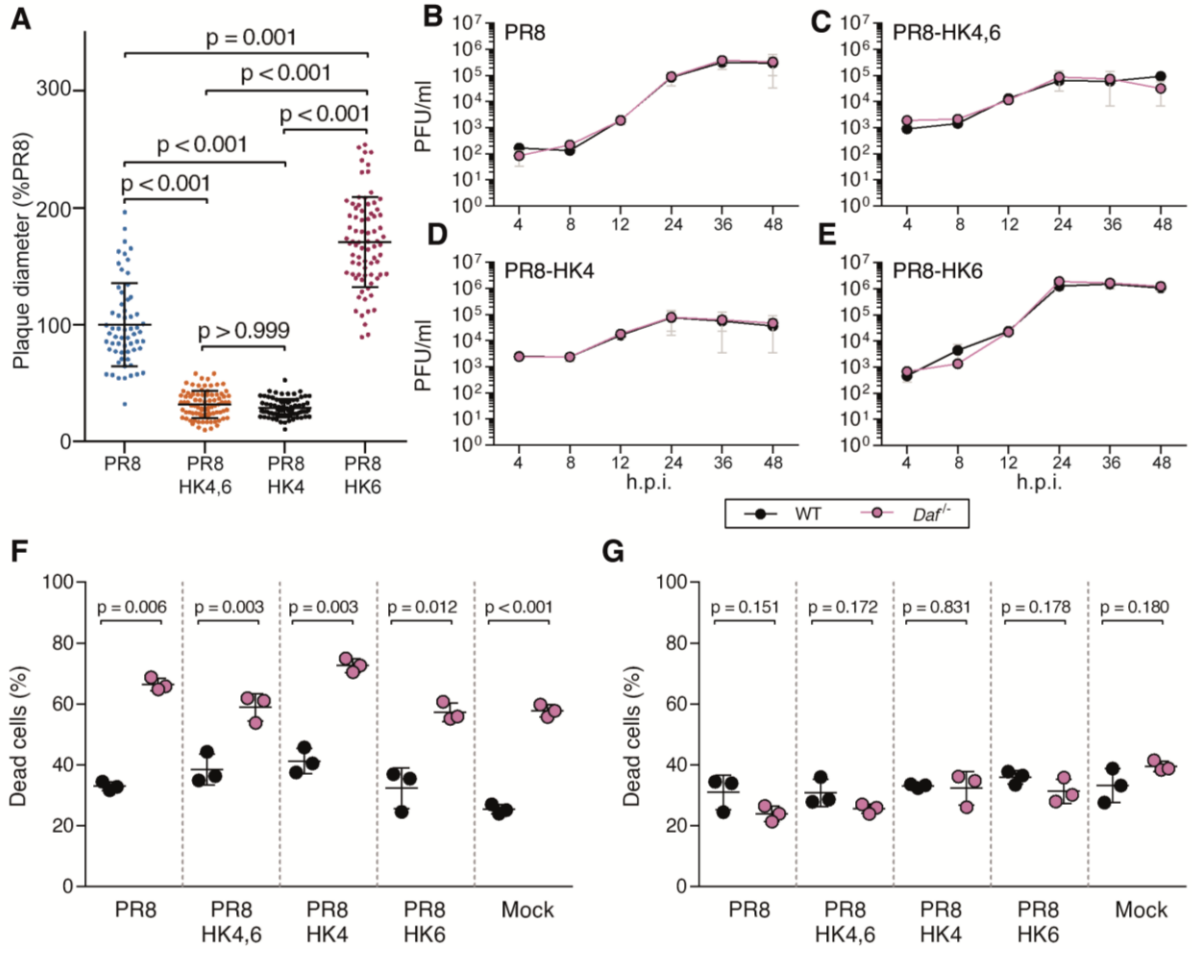

Fig. S2 – DAF does not affect replication of PR8, PR8-HK4,6, PR8-HK4 and PR8-HK6.

A: Measurement of viral plaques diameter after infection of MDCK cells monolayers. Data shown as mean±sd from two independent experiments, each corresponding to six independent infections for each virus. Each point represents an individual plaque. **B-D:** Replication kinetics of A/Puerto Rico/8/1934 (PR8) **(B)**, A/X-31 (PR8-HK4,6) **(C)**, PR8 containing the segment 4 of A/Hong Kong/1/68 (HK68) (PR8-HK4) **(C)** and PR8 containing the segment 6 of HK68 (PR8-HK6) **(D)** in mouse embryonic fibroblasts (MEFs) derived from C57BL/6J WT or *Daf*$^{-/-}$ mice at multiplicity of infection (MOI) = 0.005. Data shown as mean±SEM, from two independent experiments. Statistical analysis detailed in materials and methods.

Fig. S3

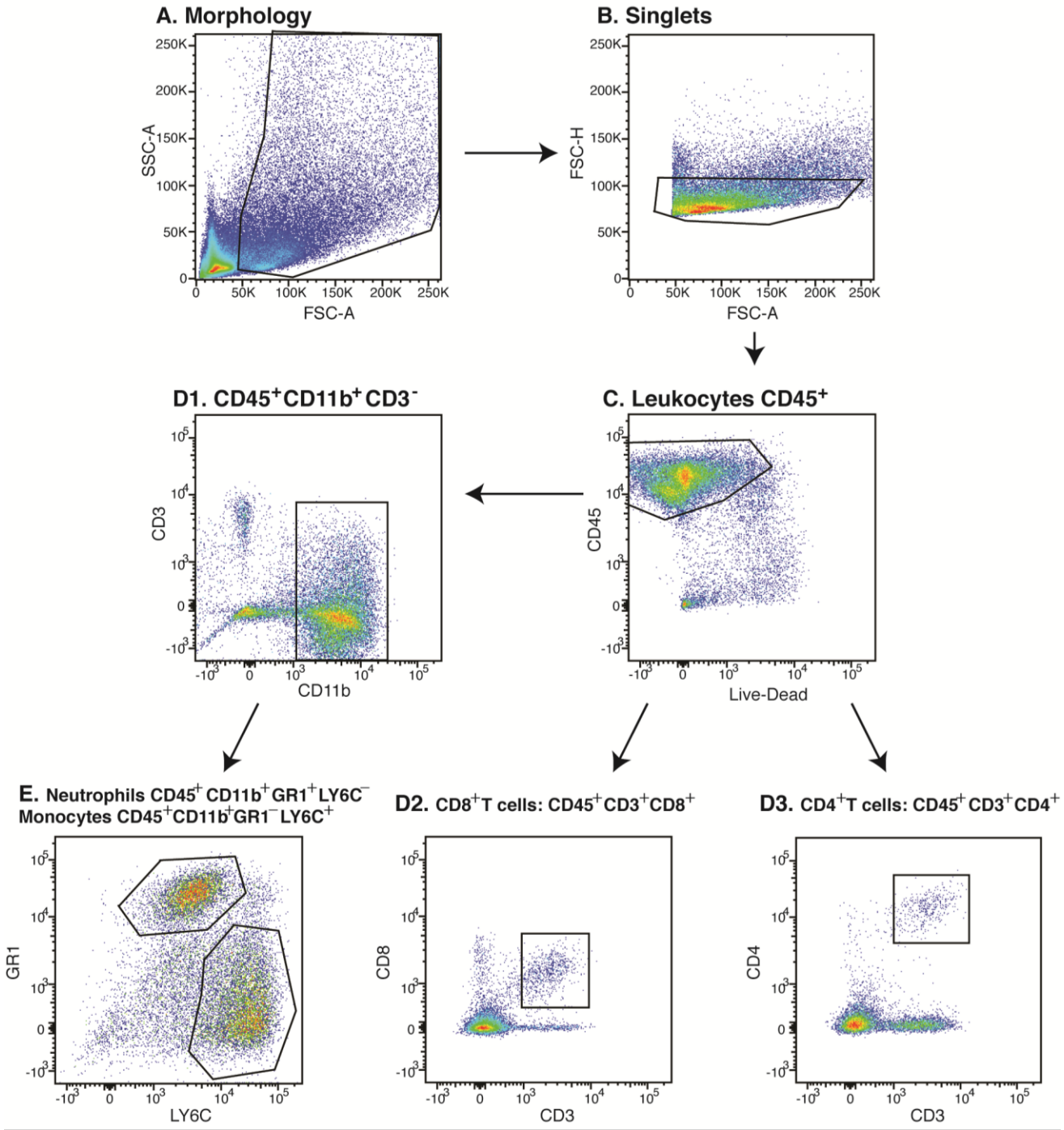

Fig. S3 – Representative flow cytometry gating strategy.

1355 **Table S1 - Histological scoring parameters.**

1356

1357

1358

IAV	C57BL/6J	d.p.i.	Interstitial inflammation median	Interstitial inflammation IQR	Alveolar inflammation median	Alveolar inflammation IQR	Perivascular/peribronchial inflammation median	Perivascular/peribronchial inflammation IQR	Bronchial exsudates median	Bronchial exsudates IQR	Bronchial epithelium hyperplasia median	Bronchial epithelium hyperplasia IQR	Edema median	Edema IQR
PR8 HK4,6	WT	3	1	0	0	1	2	0	2	2	0	0	0	0
		6	3	1	3	2	3	0	2	1	2	2	0	0
	Daf$^{-/-}$	3	1	1	0	0	2	1	1	1	0	0	0	0
		6	2	1	2	1	3	0	2	1	2	1	0	0
PR8 HK4	WT	3	0	0	0	0	1	1	1	1	0	0	0	0
		6	3	1	2	1	3	0	1	0	0	0	0	0
	Daf$^{-/-}$	3	1	1	0	1	2	1	2	1	0	0	0	0
		6	1	2	1	2	3	1	1	0	0	0	0	0
PR8 HK6	WT	3	0	0	0	0	2	2	1	1	0	0	0	0
		6	4	1	4	1	3	2	2	2	0	0	0	0
	Daf$^{-/-}$	3	1	1	0	0	3	2	1	0	0	0	0	0
		6	3	2	3	2	2	0	1	1	0	0	0	0

1359 **Table S2- Antibodies used in flow cytometry and western blot.**

1360

	Target	Brand	Catalog	Clone	Host	Diluted 1:
Flow cytometry						
CD11b/Mac1-BV605	Ms	IGC Antibody Facility	-	M1/70	Rt	100
GR1/Ly-6G-PE	Ms	BD Pharmingen	551461	1A8	Rt	200
Ly-6C-PerCPCy5.5	Ms	eBioscience	45-5932-80	HK1.4	Rt	200
CD3-FITC	Ms	IGC Antibody Facility	-	AH	Rt	100
CD4-PE-Cy7	Ms	IGC Antibody Facility	-	GK1.5	Rt	100
CD8-Pacific Blue	Ms	IGC Antibody Facility	-	YTS169.4	Rt	100
CD45-APC	Ms	BioLegend	103112	30-F11	Rt	100
CD49b/DX5-PE	Ms	BioLegend	103506	HMα2	Ah	1600
WB - Primary antibodies						
DAF	Ms	R&D Systems	AF5376	Poly	Sh	200
DAF	Hu	Abcam	ab133684	EPR6689	Rb	2000
GAPDH	Hu/Ms	Sicgen	AB0049	Poly	Gt	2000
β-actin	Hu	Sigma-Aldrich	A5441	AC-15	Ms	2000
GFP	-	Sicgen	AB0020	Poly	Gt	2000
M1	IAV	Abcam	ab20910	Poly	Gt	500
NA	IAV	R&D Systems	AF4858	Poly	Sh	500
NP	IAV	Homemade*	-	Poly	Rb	2000
NS1	IAV	Homemade*	-	Poly	Rb	500
PA	IAV	Homemade*	-	Poly	Rb	1000
PB1	IAV	Homemade*	-	Poly	Rb	500
PB2	IAV	Homemade*	-	Poly	Rb	200
WB - Secondary antibodies						
Goat IRDye 680RD	Gt	LI-COR Biosciences	926-68074	-	Dk	10.000
Goat IRDye 800CW	Gt	LI-COR Biosciences	926-32214	-	Dk	10.000
Mouse IgG IRDye 680RD	Ms	LI-COR Biosciences	926-68072	-	Dk	10.000
Mouse IRDye 800CW	Ms	LI-COR Biosciences	926-32212	-	Dk	10.000
Rabbit IRDye 800CW	Rb	LI-COR Biosciences	926-32213	-	Dk	10.000
Rabbit IRDye 680RD	Rb	LI-COR Biosciences	926-68073	-	Dk	10.000
Sheep Dylight™ 800	Sh	Rockland	613-445-002-0.5	-	Rb	10.000
Rabbit Peroxidase AffiniPure	Rb	Jackson Immunoresearch	111-035-144	Poly	Gt	25.000

*hybridomas and homemade antibodies were provided by Dr. Jonathan Yewdell and Prof. Paul Digard, respectively

1361

1362 **Table S3 - Primers used for cloning and site-directed mutagenesis.**

1363
1364
1365
1366
1367
1368
1369
1370

Primer	Sequence	For	Insert	Vector	RE
NA E229A_fw	GAGGACACAAGAGTCTGCATGTGCCTGTGTAAATG	SDM	NA	-	-
NA E229A_rv	CATTTACACAGGCACATGCAGACTCTTGTGTCCTC	SDM	NA	-	-
NA_Fw_HindIII	GCGCAAGCTTATGAATCCAAACCAAAAGAT	Cloning	NA	to pEGFP-N1	HindIII
NA_Rv_KpnI_pEGFP-N1	GCGCGGTACCGTCTTGTCAATGGTAAATGGC	Cloning	NA	to pEGFP-N1	KpnI
PR8_NA_NotI_fw	GCGCGCGCGGCCGCATGAATCCAAATCAGAAA	Cloning	NA	from pEGFP-N1 to pLEX	NotI
GFP_XhoI_rv	TCAGCTCGAGTTACTTGTACAGCTCGTCCATGC	Cloning	GFP	from pEGFP-N1 to pLEX	XhoI